UNIVERSITAT POLITÈCNICA DE CATALUNYA
BARCELONATECH
Escola d'Enginyeria de Barcelona Est

FINAL DEGREE PROJECT

Degree in Chemical Engineering

KINETICS OF DISSOLUTION OF UO_2 DOPED WITH GADOLINIUM OXIDE UNDER A WIDE RANGE OF pH

Report and Annexes

Author: Germán Peña Sánchez
Director: Ignasi Casas Pons
Co-Director: Sonia García Gómez

July 2021

Escola d'Enginyeria de Barcelona Est. EEBE

Resumen

Hoy en día, la energía nuclear es una de las fuentes de energía más importantes, generando un tercio de la electricidad en el continente europeo. Aun así, uno de los mayores problemas a los que se enfrenta es a la gestión y al tratamiento del combustible nuclear gastado (CNG). Una de las soluciones propuestas y la que mayor viabilidad posee es el almacenamiento geológico profundo (AGP). Éste consiste en almacenar el CNG a 500 metros bajo tierra, recubierto por diferentes barreras naturales y artificiales, las cuales tienen como objetivo ralentizar y evitar que el agua subterránea pueda llegar a entrar en contacto con los residuos.

Así, el proyecto tiene como objetivo el estudio de la cinética de disolución del uranio en un amplio rango de pH, especialmente alcalinos e hiperalcalinos, dada la influencia de las aguas subterráneas en el CNG. Además, se estudiará el efecto de la adición de óxido de gadolinio en la matriz de uranio debido a su uso en la industria nuclear por sus propiedades beneficiosas.

Para ello, se han sintetizado pastillas de UO_2 dopado con Gd_2O_3 5% en peso y UO_2 dopado con Gd_2O_3 10% en peso. Posteriormente, se han caracterizado correctamente las pastillas dopadas mediante las técnicas analíticas de la Microscopia Electrónica de Barrido (MEB) y la difracción de rayos X (DRX).

Estas pastillas se machacaron y se introdujeron en forma de polvo en reactores continuos de capa fina independientes entre ellos. Uno de los reactores contenía sólo UO_2, con la finalidad de determinar la influencia de gadolinio en la velocidad de disolución de UO2. Los resultados obtenidos muestran una disminución de la velocidad de disolución de UO2 cuando éste contiene gadolinio, especialmente a pH ligeramente alcalino. Este efecto de estabilización de la matriz de UO_2 debido al gadolinio es congruente con lo ya reportado en la bibliografía.

Resum

Avui en dia, l'energia nuclear es una de les fonts d'energia més importants, generant un terç de l'electricitat al continent europeu. Encara així, un dels majors problemes al que es troba front es a la gestió i al tractament del combustible nuclear gastat (CNG). Una de les solucions proposades i la que té una major viabilitat es l'emmagatzematge geològic profund (EGP). Aquest, consisteix en l'emmagatzematge del CNG a 500 metres sota terra, recobert per diferents barreres naturals i artificials, que tenen com a objectiu alentir i evitar que l'aigua subterrània entri en contacte en algun moment amb els residus.

Així, aquest projecte té com a objectiu l'estudi de la cinètica de dissolució de l'urani en un ampli rang de pH, especialment alcalins i hiperalcalins, donada la influència de les aigües subterrànies al CNG. A més, s'estudiarà l'efecte de l'addició d'òxid de gadolini a la matriu d'urani donat el seu us a l'industria nuclear per les seves propietats beneficioses.

Per aquest motiu, s'han sintetitzat pastilles amb UO_2 dopat amb Gd_2O_3 5% en pes i UO_2 dopat amb Gd_2O_3 10% en pes. Posteriorment, s'han caracteritzat correctament les pastilles dopades mitjançant les tècniques analítiques de la Microscòpia Electrònica d'Escombrat (MEB) i la Difracció de Raigs X (DRX).

Aquestes pastilles es van picar i es van introduir en forma de pols als reactors continus de capa fina independentment entre ells. Un dels reactors contenia només UO_2, amb la finalitat de determinar la influència de gadolini en la velocitat de dissolució d'UO_2. Els resultats obtinguts mostren una disminució de la velocitat de dissolució d UO_2 quan aquest té present gadolini, especialment a pH lleugerament alcalins. Aquest efecte d'estabilització de la matriu d' UO_2 gràcies al gadolini es congruent amb el que s'ha reportat a la bibliografia.

Abstract

Nowadays, nuclear energy is one of the most important energy sources, generating one third of the electricity on the European continent. Although, one of the major issues it faces is the management and treatment of the spent nuclear fuel (SNF). One of the proposed solutions and that has a great viability is the Deep Geological Repository (DGR). It consists on the storage of the SNF 500 meters underground, recovered by a multibarrier system, formed by natural and artificial barriers, which aim to slow down and prevent groundwater from getting in contact with the nuclear waste.

Thus, this project aims to study the kinetics of dissolution of the uranium in a wide range of pH, especially alkaline and hyperalkaline, given the influence of groundwater on SNF. In addition, the effect of adding gadolinium oxide into the uranium matrix due to its use in the nuclear industry for its beneficial properties will be studied.

In order to achieve it, pellets with UO_2 doped with Gd_2O_3 5% wt. and UO_2 doped with Gd_2O_3 10% wt. have been synthesized. Then, doped pellets have been correctly characterized by Scanning Electron Microscopy (SEM) and X-Ray Diffraction (XRD) analytical techniques.

Pellets were crushed and fed in powder form into independent continuous thin-film reactors in powder from. One of the reactors was filled only with UO_2, in order to determine the influence of gadolinium on the UO_2 dissolution rate. The results show a decrease in the dissolution rate of UO_2 when it contains gadolinium, especially at slightly alkaline pH. This stabilization effect of the UO_2 matrix due to gadolinium is congruent with what has already been reported in the bibliography.

Agraïments

En primer lloc voldria agrair al meu tutor, l'Ignasi, per obrir-me les portes d'aquest món completament desconegut per mi i donar-me l'oportunitat de poder realitzar aquest TFG. També, a la Sonia, co-directora, per tota la seva ajuda, fos quan fos, i crear un gran ambient durant els matins o tardes de laboratori al llarg d'aquests mesos.

M'agradaria agrair a la meva família, que sempre m'ha recolzat en cadascuna de les decisions que he pres en la meva vida i sempre ho faran. Finalment, a cada persona que s'ha interessat en com avançava dia a dia el projecte i m'ha donat ànims per continuar.

Acronym list

BET: Brunauer- Emmett- Teller
CTS: Centralized Temporary Storage
DGR: Deep Geological Repository
ENRESA: Empresa Nacional de Residuos Radioactivos
HLW: High-level waste
ICP-MS: Inductively Coupled Plasma- Mass spectrometry
ILLW: Intermediate and low-level waste
ITS: Intermediate Temporary Storage
LEU: Low-enriched uranium
NAF: Neutron-Absorbing Fuel
NDR: Normalized Dissolution Rate
NPP: Nuclear Power Plants
RN: Radionuclides
SA: Surface area
SEM: Scanning Electron Microscope
SNF: Spent Nuclear Fuel
XRD: X-ray Diffraction

Table of contents

1. Introduction

Today, the 30% of generated electricity in Europe comes from nuclear energy and over 430 commercial nuclear power reactors in 31 countries provide just over 10% of the world's electricity. [1]

As all industries and energy-producing technologies, the use of nuclear energy results in some waste products. In Spain, the waste management solution is different according to their radioactivity: low, very low and intermediate-level waste and high-level waste. The first group contains mostly short-lived radioactivity and can be handled safely with simple precautions, whereas the second group is mainly constituted by spent nuclear fuel (SNF) and has a long-lived radioactivity. [1][2]

In the first group of waste types, the Spanish legislation requires the transfer of this material from its producer or holder to Enresa, whatever the form or characteristics of the material. It can be stated that Spain has a global resolution on the nuclear waste, having a management system that is well-equipped and operates in a structured way. Thus, every nuclear plant could prepare and condition the nuclear waste in order to be transferred to Enresa for their storage in the CA El Cabril. In case the plant could not condition it, the producers would deliver it to this company and it is this one who performs the treatment prior to the storage. [2]

Figure 1.1. CA El Cabril facilities and the storage cell of the nuclear waste.

Regarding the waste management of high-level waste, currently, it is stored both in Individualized Temporary Storage (ITS) or Centralized Temporary Storage facilities (CTS), which can be located whether inside or outside the nuclear power plant or on the surface or few meters deep. It also has the purpose of refrigerate and cool down the spent nuclear fuel from 50 to 100 years in some countries. [2][3]

Thus, it has been internationally accepted that the safest and most economically viable option to finally dispose the SNF is the Deep Geological Repository (DGR). It is based on the protection and confinement of nuclear waste, which will be stored underground. Finland seems to be the world's first country to construct a permanent geological repository for SNF and high-level radioactive waste. It is expected to commence operations in 2025, whereas in Spain is scheduled to start operating in 2073. [2]

1.1 Deep geological repository (DGR)

The DGR's main concept in Europe is based on the isolation and confinement of the nuclear waste in deep geological formations. Therefore, the geological disposal concepts studied are based on a multibarrier system that prevents or delays the underground water from coming into contact with the nuclear waste, which is inside, and limit any subsequent dispersal that could be released in order to avoid radioisotopes back to the biosphere. [4] [5]

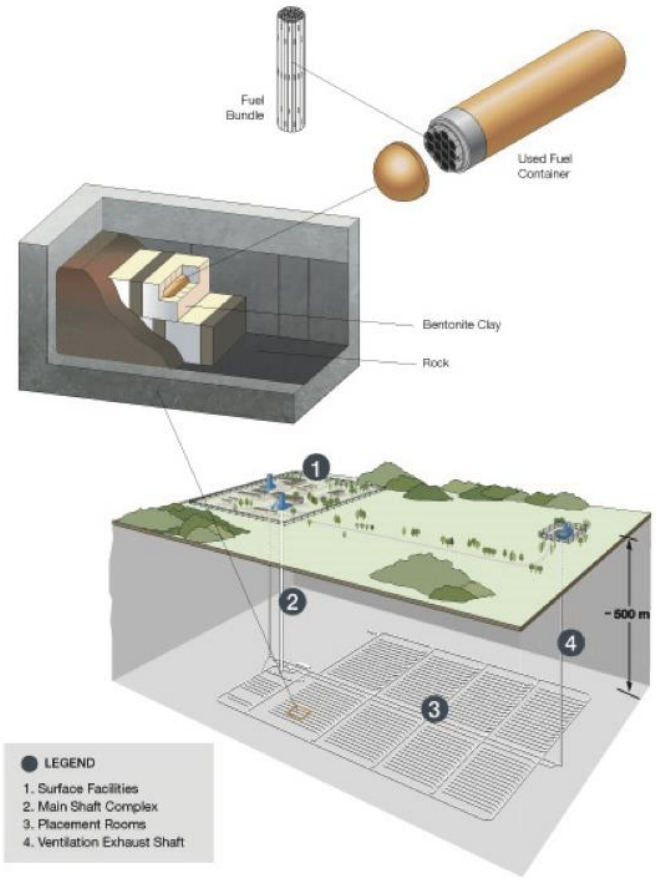

Figure 1.2. Summary of a DGR. [4]

As seen in the Figure 1.2, the multibarrier system design is formed by different impediments, at a depth underground of approximately 500 meters, where each barrier delays the exposition of the SNF to water. Regarding this, the first impediment is the SNF itself, which is composed of a UO_2 matrix and when ground water gets in contact with the spent fuel, the UO_2 will partially control the release of the radionuclides (RN) to the ground water. [6]

Then, the nuclear waste is stored in a metallic tube made of zirconium alloy known as Zircaloy and has a very low corrosion rate. During the irradiation process, some neutrons are captured by metallic atoms of the fuel bundle.

The third impediment consists of a metallic container where all the previous SNF is introduced. Its main objective is to contain and isolate the nuclear fuel. This barrier is expected to improve the handling, to avoid physical damage to the nuclear waste and to improve the heat transfer, decreasing the temperature of the SNF.

Finally, the used fuel container will be surrounded by a clay barrier made of bentonite to delay the contact with water. This material is considered to be an appropriate barrier because it has the characteristic of increasing its volume in contact with water sealing any possible crack or pore. This property will help to increase the time that water needs to pass through all the barriers before getting in contact with the SNF. The clay will also provide the groundwater with some properties that might have an effect on the SNF alteration processes, depending on the composition. In addition, the clay barrier itself might adsorb part of the RN dissolved in the ground water. In addition, cement will also be used in order to give stability to the structure.

The emplacement and the minerals of the geological location will be the final barrier. The geological formation will modify the groundwater composition and control the water flow. Therefore, as mention before, it must have specific characteristics regarding its mechanical stability, enough thickness to protect the DGR, thermal conductivity, water permeability and homogeneity. [7]

1.1.1 Alteration of barriers in the DGR

The groundwater composition will change after the interaction with the different barriers present in the DGR before getting in contact with the SNF. The three main types of geological formation are identified as a function of their composition to host the repository: granitic, salt or clay bedrocks. Since the bedrock will be in contact with the clay barrier, some studies have determined the ground water composition resulting from the combination of both. The composition of the water obtained from the water saturation in contact with granitic bedrock and the bentonite barrier is shown in Table 1.1. [8]

Table 1.1. Composition on the groundwater. [8]

Species	Cl^-	SO_4^{2-}	HCO_3^-	Na^+	K^+	Ca^{2+}	Mg^{2+}	pH
Concentration ($mmol \cdot dm^{-3}$)	93.9 ± 9.4	45.2 ± 4.5	0.9 ± 0.1	117.9 ± 11.8	1.1 ± 0.1	15.4 ± 1.5	17.3 ± 1.7	7.6 ± 0.2

Moreover, although hardened cement is generally slow to react with groundwater unless it is porous, in case both could get in contact, could form and release calcium and silicate hydrates, which lead to hyper alkaline conditions (pH concentrations values as 13,5-14). [9]

Also, in this hypothetical situation, the metallic container could be corroded in contact with the ground water. This container is made of stainless steel, which may be corroded to produce hydrogen and iron oxides through the following reactions [10]:

$$3\,Fe\,(s) + 4\,H_2O \Leftrightarrow Fe_3O_4\,(s) + 4\,H_2(g) \quad (1)$$

$$Fe(s) + 2\,H_2O \Leftrightarrow Fe_2+ + H_2(g) + 2OH^- \quad (2)$$

Thus, some of the products obtained from the previous reactions might be dissolved in the aqueous phase which could provide the groundwater with reducing properties. Those reducing agents would influence the alteration of the SNF in contact with the water. For instance, $Fe^{2+}(aq)$ was determined to inhabit the corrosion of the SNF and the RN release. Also, the presence of $H_2(g)$ in the SNF is proved to decrease the dissolution of the SNF matrix, which might reduce the RN release to the groundwater. [11]

1.2 Spent Nuclear Fuel

There are a number of different types of fuel, but to maximize energy output are predominantly uranium based, mainly UO_2, which consists of two isotopes of interest: ^{235}U (0,72 atomic %), which is fissile, and ^{238}U (99,27 atomic %), which is fertile. Although, for most reactors the uranium fuel is enriched from 3 to 5% ^{235}U as a low-enriched uranium (LEU) fuel. [12][3]

Although the nuclear process does not yield CO_2 or greenhouse gas emissions, the primary waste form resulting from a nuclear energy production is the Spent Nuclear Fuel (SNF). The SNF used in the Spanish Nuclear Power Plants (NPP) is UO_2 compressed and synthetized into cylindrical shaped pellets, which are introduced in a Zirconium alloy cladding. [12][3] Thus, at the end of the fuel's useful life in the reactor, about 96% of the SNF is still UO_2. [3] The remaining consists of fission products, activation products or minor actinides, which occur in different phases:

- Fission product gases, such as Xe, I and Kr, occur as finely dispersed bubbles in the fuel grains.
- Metallic fission products, such as Mo, Tc, Ru, Rh and Pd, form immiscible metallic precipitates (ε- particles).
- Fission products form oxide precipitates of Rb, Cs, Ba and Zr.
- Fission products elements, such as Sr, Zr, Nb and lanthanides can form solid solutions with UO_2.
- Trans uranium elements can substitute for U in the UO_2.

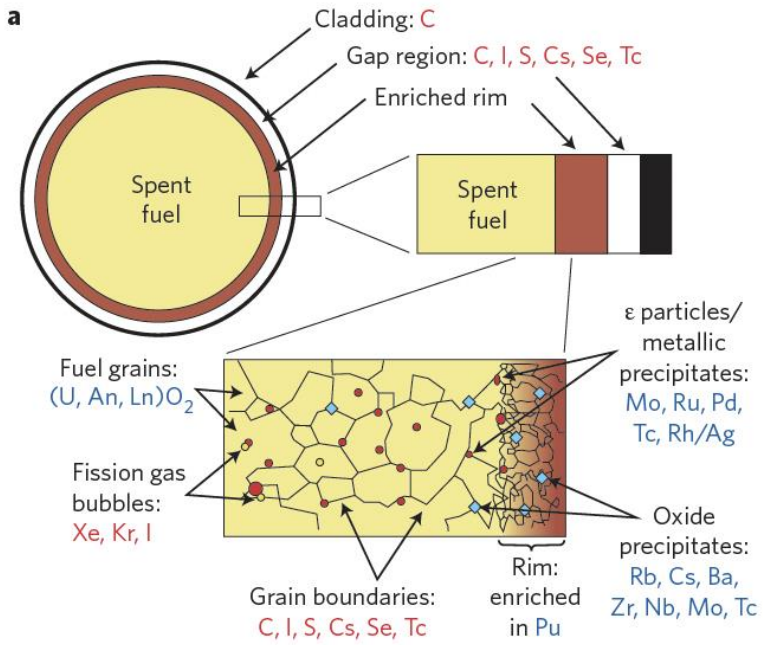

Figure 1.3. SNF microstructure and distribution of the fission products. [3]

Elements distribution in SNF granules is not homogeneous as shown in Figure 1.3. Three different important parts can be differentiated:

- Core: The core of the SNF is the centre part of the pellet. Most of the RN's inventory retained in the fuel is dissolved in the UO_2 matrix and, therefore, the matrix will govern their release to the environment. The RN that are expected to be fully dissolved in the matrix are mainly lanthanides and actinides due to their similarities with uranium and their solubility in the UO_2.
- The enriched rim, located in the periphery of the pellet, close to the gap region and the cladding. This region presents higher concentration of Pu than in the central part of the fuel pellet.
- The gap region is located between the cladding and the fuel pellet. This region is where the fission gas is accumulated: between the core of the nuclear fuel pellet and the periphery.

As a result, the gap region is rich in fission gas and other volatile elements like ^{129}I, ^{137}Cs, ^{135}Cs, ^{36}Cl, ^{79}Se and possibly ^{126}Sn. It also might contain non-volatile and partially segregated RN like ^{14}C. [13]

Otherwise, elements in red are released rapidly on first contact with water, while elements in blue are released more slowly as the UO_2 matrix corrodes. [3]

1.2.1 Evolution of the Spent Nuclear Fuel

The initial level of radioactivity of the irradiated fuel is very high, caused mainly by the presence of the 3 to 4 at. % of fission products (for example ^{131}I, ^{137}Cs and ^{90}Sr) and activation products (^{60}Co, ^{63}Ni), with a longer-lasting contribution from long-lived elements, such as ^{239}Pu, ^{237}Np or ^{241}Am). [3]

One year after discharge the fuel from the nuclear reactor, the radiation dose will be 106GBq/MT fuel or higher, which means a person exposed to this level of radioactivity at a distance of one meter would receive a lethal dose in less than a minute; hence spent fuel must be handled remotely. This increase in radioactivity is caused by the presence of 3 to 4 at. % of fission products, transuranium elements and activation products in the metal spent fuel assemblies. [12]

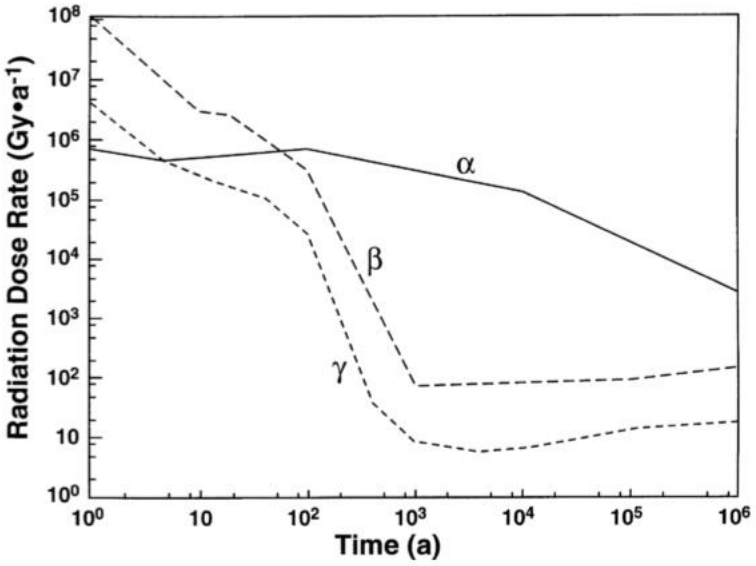

Figure 1.4 Radiation dose rates as a function of time. [14]

The very penetrating ionizing radiation (α and β) comes mainly from the short-lived fission product with half-lives of about 100 years. Due to the radioactivity decay, the SNF evolves with time in composition and radiotoxicity. As the short-lived isotopes decay, the radioactivity of the waste also decreases as it can be observed in Figure 1.4. Then, the radiation dose will be provided by α-radiation emitted from the fuel by isotopes of Pu, Am, Np and U mainly. Finally, the radiation emitted from the fuel will reach the same value as natural uranium minerals millions of years after the discharge.

Only the most stable isotopes (such as ^{99}Tc (210,000 years), ^{79}Se (1.1 million years), ^{135}Cs (2.3 million years) or ^{129}I (16 million years)) will remain in the SNF after long periods of time. Each long-lived RN has its relative importance for the performance assessment depending on their mobility under the DGR conditions. For instance, those elements with high solubility and high mobility are likely to be released rapidly when the SNF gets in contact with groundwater. [12] [5]

At the time when the ground water gets in contact with the SNF, which is thousands of years after the DGR closure depending on the lifetime of the barriers, the radiation emitted is expected to be mainly due to the α-radiation, as it can be observed in Figure 1.4. [5]

1.2.2 Doped nuclear fuel

The most important application of doped uranium dioxide for the nuclear industry is the production of neutron-absorbing fuel (NAF), which is used to reduce the reactivity of fresh fuel assemblies at the beginning of life's reactor in order to optimize it. Gadolinia (Gd_2O_3) is very suitable for the production of NAFs due to the large neutron-absorption cross section of ^{155}Gd and ^{157}Gd isotopes.

Gadolinium-doped UO_2 pellets and their importance in the nuclear industry has increased due to the recent trend to achieve higher burnups (measurement of how much energy is extracted from a primary nuclear fuel source). From this viewpoint, when the UO_2 matrix is doped with Gd (maximum 10% wt.) basic properties and its behaviour are modified on the thermodynamic, thermal and physical properties and the phase stability. Although Gd is well below the solubility in UO_2, some Gd ions segregate to grain boundaries of the matrix. [15] [16]

The main reason the matrix is doped at maximum 10% wt. is because it was shown that up to 10% wt. of Gd_2O_3 content, it has no significant effect on the theoretical density of the fuel. Figure 1.5 shows the effect of Gd_2O_3 content on the sintered density of material as observed. [17]

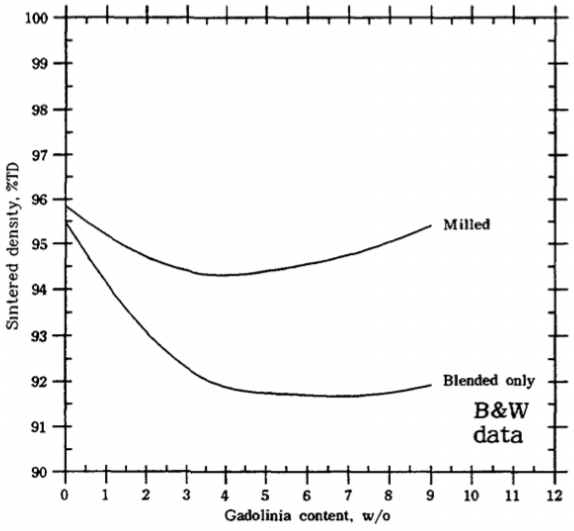

Figure 1.5. Gadolinia content on the sintered density. [17]

1.3 Spent Nuclear Fuel interactions

1.3.1 Near field conditions

In case the different barriers fail and the underground water gets in contact with the SNF, the dissolution and interactions will take place.

The main processes affecting and controlling the dissolution of UO_2 in spent nuclear fuel are schematically illustrated in Figure 1.6. The dissolution and the alterations of the spent nuclear fuel could be described as a sequence of four processes: [12]

- Groundwater radiolysis in a long term by the alpha radiation principally (as beta and gamma in a short term will be the strongest radiation but after 1000 years will be insignificant). Under reducing conditions, the radiolysis can create oxidizing conditions at the surface of the SNF. Whereas, under oxidizing conditions, the radiolysis will be less important.
- Oxidants that are produced or already present have a strong tendency to oxidize the surface of UO_2 to UO_{2+x} that will contain U(VI).
- The oxidized U(VI) at fuel surface is dissolved by complexing ligands present in groundwater. The initial composition may be modified by concentration during evaporation or reaction. Uranium (VI) has a strong tendency to form complexes in solution, in particularly the carbonates. Main oxygen-containing ligands in groundwaters are bicarbonate ($HCO3^-$) and hydroxide (OH^-).
- The U(VI) dissolution continues until the saturating point, where might result in the precipitation of secondary U(VI) phases under oxidizing conditions.

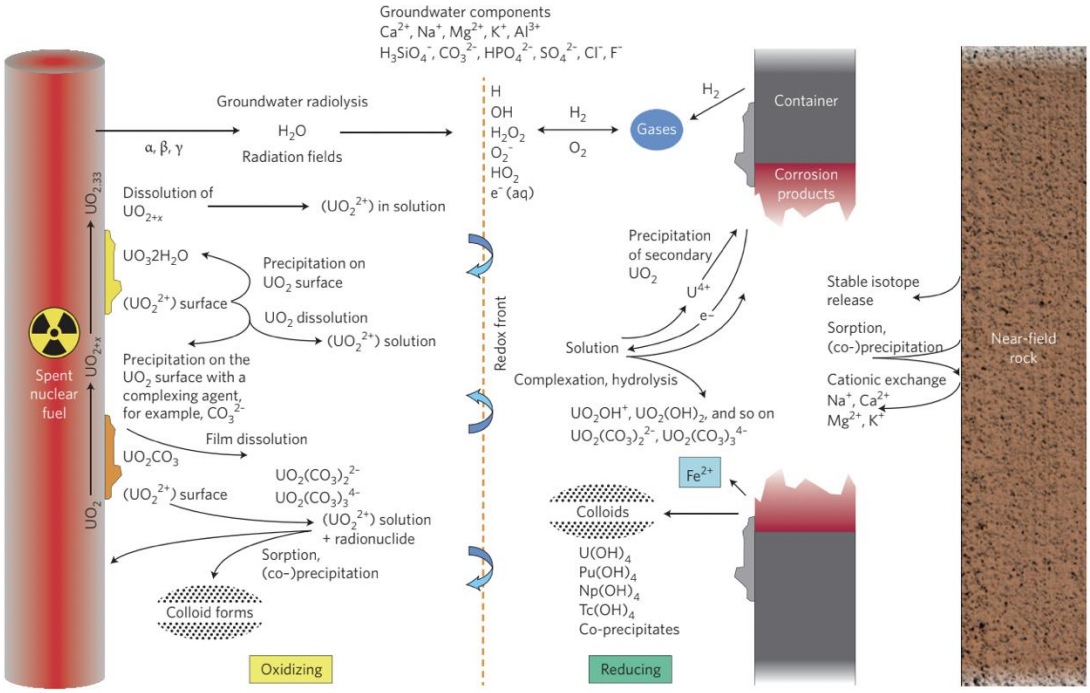

Figure 1.6. Scheme of the chemical process involved in the near field conditions [3]

Thus, the main objective is to examine the influence in the behaviour that the groundwater might have when getting in contact with uranium and gadolinium in the repository. As mention above, all types of nuclear wastes (doped and undoped) will be stored inside, so it is important to know the aspects that will influence the SNF.

1.3.2 pH effect

The positive dependence on $[H^+]$ between pH 3 and 7, as shown in Figure 1.7, shows that the dissolution rate of UO_2 is favoured in this range by the presence of H^+ ions in solution. Hence, it is proposed the following mechanism for the UO_2 dissolution under reducing conditions: [18]

- Step 1: Oxidation of the surface of the solid

$$> UO_2 + ½\ O_2 \Leftrightarrow > UO_3 \qquad (3)$$

- Step 2: Surface co-ordination of H^+ (favoured at acidic pH)

$$> UO_3 + H^+ \Leftrightarrow > UO_2(OH^-) + (aq) \qquad (4)$$

- Step 3: Surface co-ordination of H_2O (favoured at neutral- alkaline pH):

$$> UO_3 + H_2O \Leftrightarrow UO_2(OH)_2\ (aq) \qquad (5)$$

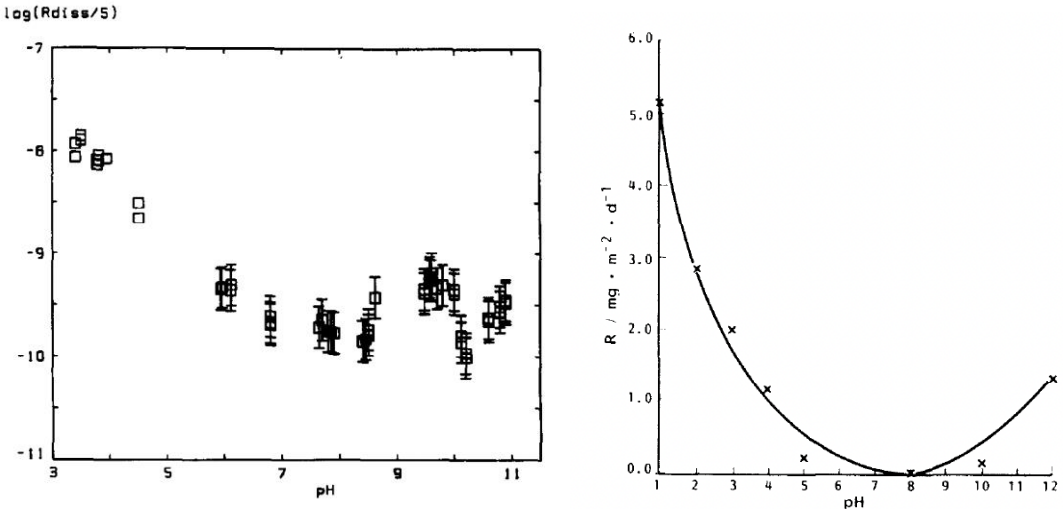

Figure 1.7. Evolution of UO_2 dissolution versus pH. [19]

These results indicate that this dissolution can be explained from a surface complexing mechanism, where at low pH values the concentration of uranium will be higher, which implies a higher dissolution rate too and that is what can be observed experimentally. As it can be seen from Figure 1.7, at acidic concentrations of H^+, as the pH increases the dissolution rate is inversely proportional, it decreases. This dependence is not so evident at neutral and alkaline pH values, where dissolution rate in this range is relatively low and similar for the different experiments. It reaches the minimal value between pH value from 5 to 10.

1.3.3 Carbonate effect

Carbonate is present in groundwater and, therefore, the influence that could have in the UO_2 matrix needs to be studied.

De Pablo (1999) proposed the following mechanism in order to describe this influence [20]:

- Step 1: Oxidation of the surface of the solid

$$> UO_2 + ½\ O_2 \Leftrightarrow > UO_3 \quad (6)$$

- Step 2: Surface co-ordination of U (VI) by HCO_3^-

$$> UO_3 + HCO_3^- \Leftrightarrow > UO_3 - HCO_3^- \quad (7)$$

- Step 3: Detachment (dissolution) of the products species:

$$> UO_3 + HCO_3^- \Leftrightarrow \text{“U (VI)(aq)”} \quad (8)$$

Later, in the study performed by Shoesmith (2000), this mechanism was adapted, in which they concluded that the influence of carbonate was dependent of its concentration. Four different scenarios were proposed [14]:

- Absence of carbonate: Corrosion products could accumulate and suppress the dissolution rate.
- Concentrations lower than 10^{-3} M: The deposition of corrosion products is avoided due to the increase of UO_2^{2+} solubility.
- Intermediate concentrations (10^{-3} to 10^{-1} M): HCO_3^- / CO_3^{2-} is kinetically involved, via the formation of surface intermediates, in the solution process.
- For high concentrations: The presence on the surface of a secondary phase limits the rate of dissolution and the reaction becomes much less dependent on carbonate concentrations.

Therefore, the conclusions are that the presence of HCO_3^- in granitic groundwater will enhance the solubility of uranium. Then, experiments will be performed with intermediate concentrations to simulate the conditions. [21][14]

1.3.4 Doping with Gd effect

A number of studies have been made regarding the influence of gadolinium on the uranium dioxide, for example in [16] or in [21] addition of Gd to the fuel appears to have a stabilizing effect on the UO_2 matrix by reducing the availability of oxygen vacancies (O_v) required to accommodate oxygen during oxidation. Then, it was concluded that the increased dopant concentration reduced the oxidative dissolution rate up to an order of magnitude at room temperature over the tested dopant range. [22]

Therefore, the importance of this project is based on the reduced bibliography that exists on the Gd effect. As mention before, some other researches are about the gadolinium influence on the temperature or pressure, whereas, this project discuss about the influence of Gd on the uranium dioxide under a wide range of studied pH. [22] [16]

2 General objetives

The main objective is to study how UO_2 will behave under the conditions described. This project contributes studying the influence of gadolinium in the kinetics of dissolution of uranium dioxide and the influence of pH. Therefore, the specific objectives are summarized below:

- To synthesize and characterize UO_2-Gd_2O_3 doped pellets.
- To assemble and start-up a continuous thin film reactor to study the kinetics of dissolution of the uranium and gadolinium under a wide pH range.
- Evaluate and determine the influence of gadolinium and the pH on the UO_2 dissolution rate.

3 Experimental

3.1 Synthesis of gadolinium doped with UO_2

Two different types of pellet were prepared with 5% and 10% in mass to determine the influence of Gd. The following diagram block was inspired in the study that Baena did in 2015. [16]

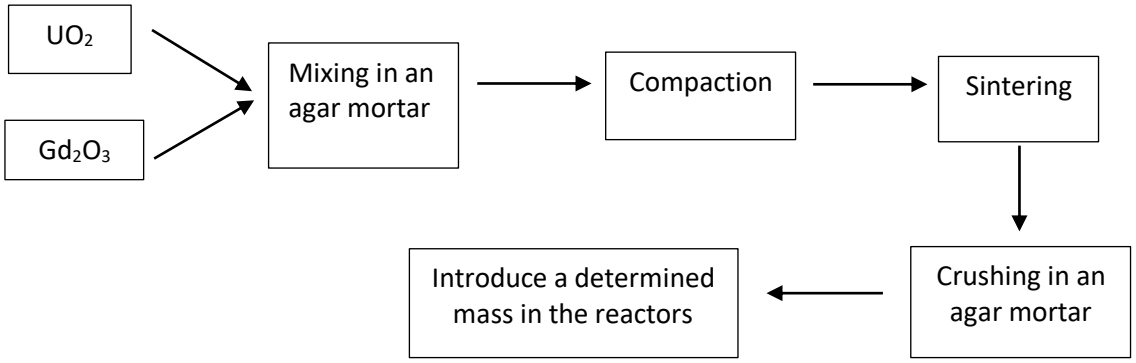

Figure 3.1. Diagram block

Thus, the different masses of uranium oxide and gadolinium oxide were prepared and mixed in an agar mortar. Then, the mixture was compacted using a press for a minute applying a force from 6 to 7 tons. The following step was the sintering process, which was carried out in a Horizontal tube furnace ST196030 HG from Hobersal as shown in Figure 3.2. It reaches a temperature of 1740ºC for 8h, increasing the temperature 5ºC per minute. It works in a reducing atmosphere with 95% in volume Ar(*g*) and 5% in volume of H_2 (*g*) to prevent U(IV) to U(VI) oxidation. Joints are placed in the furnace tube in order to have a constantly water recirculation due to the high temperatures.

Later, pellets will be characterized using SEM and XRD techniques that will be explained in section 4 and results will be shown in section 5.

Figure 3.2. Horizontal tube furnace ST196030 HG from Hobersal

3.2 Dissolution rate determination

The main objective of the project is to study the kinetics of dissolution of uranium and gadolinium under different pH conditions in a range from 2 to 13.

The dissolution rate determination is based on the uranium concentration at steady state. The amount of uranium dissolved depends on the reaction time, which is related to the residence time of the test solution in the reactor, given by: [18]

$$t = V / Q \tag{9}$$

where V is the volume of the solution in contact with the solid phase and Q is the flow rate. Dissolution rate value (mol/s) for uranium and gadolinium is calculated using the following equations:

$$r_{diss\ U02} = Q \cdot [\ U(VI)\ ] \tag{10}$$

$$r_{diss\ Gd2O3} = Q \cdot [\ Gd\ ] \tag{11}$$

It is necessary to be precise in the different values (weight of solid in the reactor, the specific surface area…), in order to compare the results obtained and normalize all the rate dissolution values that will be useful in other research. To calculate this parameter, it is used the normalized dissolution rate (NDR):

$$\text{NDR } UO_2 = \frac{(Flow\ Rate)\cdot(U\ concentration\ in\ Leachate)}{(Sample\ Weight)\cdot\left(\frac{grams\ U}{grams\ UO2+grams\ Gd}\right)\cdot(Specific\ SA)} \quad (12)$$

$$\text{NDR } Gd_2O_3 = \frac{(Flow\ Rate)\cdot(U\ concentration\ in\ Leachate)}{(Sample\ Weight)\cdot\left(\frac{grams\ Gd}{grams\ Gd+grams\ UO2}\right)\cdot(Specific\ SA)} \quad (13)$$

Where SA is the surface area and the specific fraction of U and Gd per sample, which takes into account Gd and O weight. The dissolution rates presented were taken after steady state was established in order to eliminate effects such as initial oxidation and release of fines. [23]

3.2.1 Continuous reactors: The thin film reactor

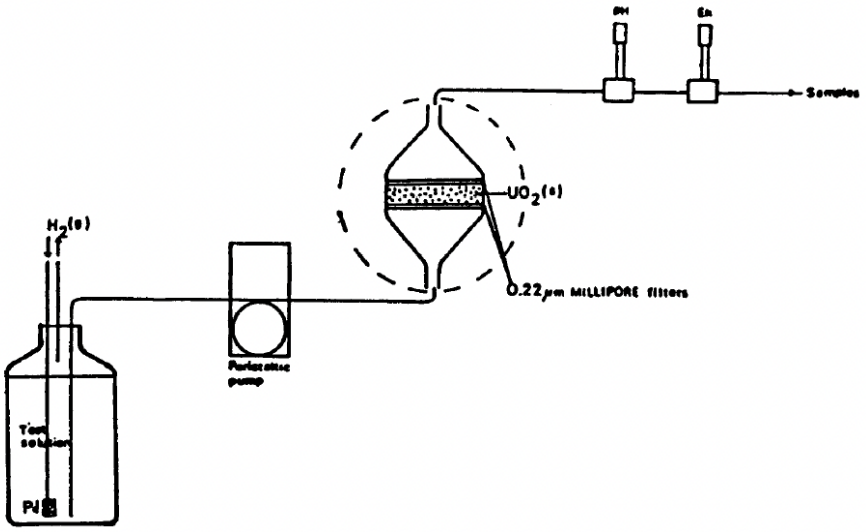

Figure 3.3. Experimental scheme of a continuous thin film reactor. [18]

The experimental system used is a continuous thin film reactor (Figure 3.3). In this system, the solid phase is contained in a reactor where the test solution is continuously pumped through it. Using a thin layer of solid ensures an optimum contact between both solid and liquid phases, as the main objective is to prevent the saturation and avoid the undesired secondary phases formations. Also, it minimizes the diffusion through the solid that can arise when a thicker layer is used as well as the contact time is reduced between both phases.

Once the solid is enclosed into the reactor, without any pre-treatment, no further manipulation is required, because a new experiment is started just by changing the conditions on the input test solution. The problems concerning the presence of highly reactive phases different from the bulk uranium dioxide are eliminated during the first hours of the experiment. The more soluble phases are dissolved out of the reactor in the initial stage, giving a high initial concentration of the dissolved products in the output solution. This is shown in Figure 3.4, a study done by Bruno in 1990, in which one must be ensured that the uranium concentrations measured actually correspond to steady state, reached approximately after 24 hours after the system is settled up. [18]

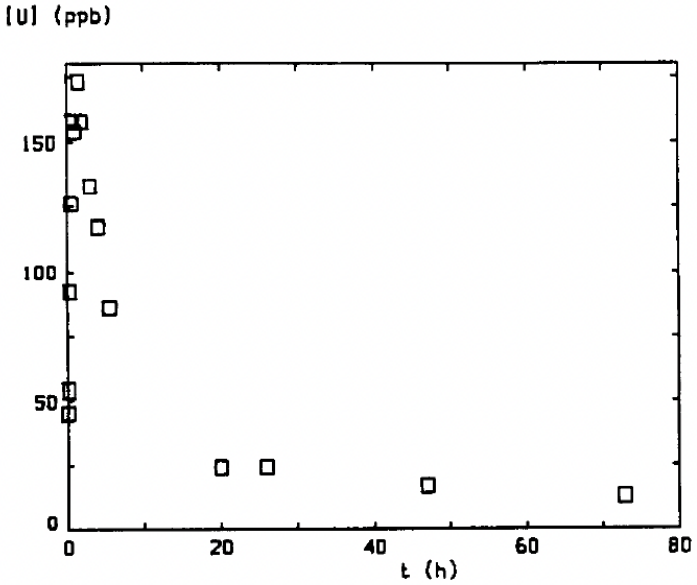

Figure 3.4. Uranium concentration since the experiment started [18]

Once the pellets have been sintered and characterized, it is necessary to sieve them in order to get a sample with a 50-75 µm particle diameter. Later, the solid was analyzed by BET and introduced in the reactors.

Then, a known weight of solid, approximately 0.16 grams with a 50-75 particle diameter, was introduced into the reactor between two MILLIPORE filters (diameter: 13 mm) to ensure that only the concentration of dissolved uranium is measured.

Therefore, Reactor A is filled with pure UO_2, Reactor B consists of UO_2 doped with 5% Gd_2O_3 and finally, Reactor C of UO_2 doped with 10% Gd_2O_3.

All test solutions were prepared using ultrapure water from a Millipore Milli-Q system in a pH range from 2 to 13. Each solution represents a new experiment and it is introduced into a bottle to minimize contaminations. Solutions were also prepared with $5 \cdot 10^{-3}$M $NaHCO_3$ (99.7% Merck) to simulate the groundwater composition and $NaClO_4 \cdot H_2O$ (98% PanReac) in order to keep a constant ionic strength of 0,1M. To adjust the pH in alkaline solutions it was used NaOH (99.9% PanReac) and in acidic solutions it was used HCl (37% PanReac).

A stream of nitrogen is also pumped into the bottle constantly in order to avoid CO_2 intrusion. Three different effluents from the test solution feed each reactor. All the connections are perfectly wrapped with film to avoid any leak.

As mentioned above, depending on the pumping speed the residence time on the reactor will change. Thereby, when the pumping speed is slow (Q is low) the residence time will be higher and the uranium concentration will increase. On the other hand, when Q is higher, the residence time and the concentration will decrease.

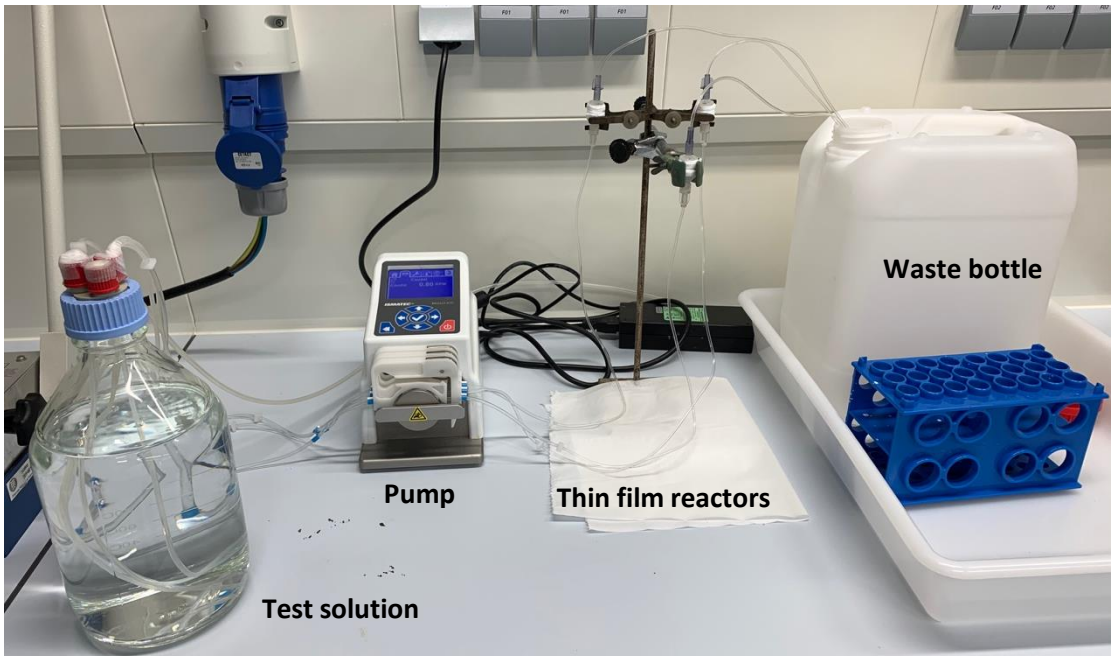

Figure 3.5. Experimental system used in the laboratory

Then, as Figure 3.5 shows, once the solution has gone through the reactors it arrives to either the waste bottle or the different tubes test, as some samples are taken periodically every day for a fixed period depending on the pumping speed. The process consisted of the addition of 0.2 mL of concentrated NH_3 to the test tubes, as to ensure that the uranium remained in solution rather than being deposited on vial walls. Then, samples were collected and once the time has elapsed, 5mL of Milli-Q water were added, in order to reduce the concentration of salts in the sample for ICP-MS measurement. [23]

Finally, uranium and gadolinium concentrations from the samples were analysed in the ICP-MS. Then, using the equations (10) and (11) the dissolution rate value is obtained and using the equations (12) and (13) the normalized value is obtained.

4. Analytical Techniques

As mentioned before, pellets were characterized using SEM and XRD, powder characterization for the kinetics study were performed with BET and the measurement of the uranium and gadolinium concentration were performed by the ICP-MS technique.

4.1 Scanning electron microscopy (SEM)

SEM is a technique that produces images of a sample by scanning it with a beam of electrons. The electrons interact with the different atoms presented at the sample surface, producing various signals that reveal information on the sample surface morphology and composition. [24]

EDX spectroscopy is involved in the detection of elemental compositions of substance by using scanning electron microscope. EDX is able to detect elements that possess the atomic number of higher that boron and these elements can be detected at concentration of least 0,1%. When two methods are combined, the samples interact with the beam and produce characteristic X-rays. Due to the principle that none of the elements have the same X-ray emission spectrum, they can be differentiated and measured for its concentration in the sample. The depth from where the X-rays originate depends on the material and the used primary electron beam energy. For typical primary energies of 10 to keV it is in the µm.[24]

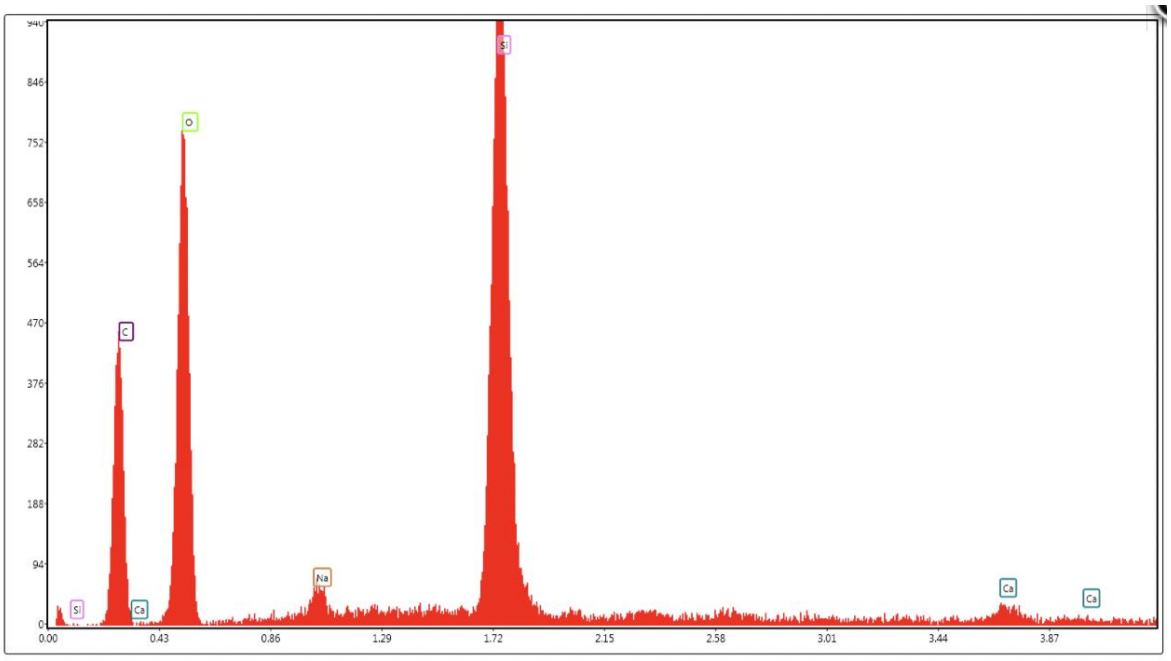

Figure 4.1. Example of composition that SEM-EDX represents.

4.2 X- Ray Diffraction (XRD)

X-ray diffraction analysis (XRD) is a technique used in materials science to determine the crystallographic structure of a material. XRD works by irradiating a material with incident X-rays and then measuring the intensities and scattering angles of the X-rays that leave the material.
It is used in mineralogy and materials engineering sectors, especially in metallurgy and ceramics. It is used to determine the samples purity, quantitative analysis of a compound within a material, identify phases and determine phase diagrams as determine the crystalline structures. [25] [26]

X-ray diffraction occurs when a beam, which has a determined wavelength, interacts with a crystalline substance. It is based on the coherent dispersion of the X-ray beam in contact with matter and constructive interference of waves that are in phase dispersed in certain directions of space. [25] [26]

4.3 Inductively coupled plasma- mass spectrometry (ICP-MS)

Inductively coupled plasma– mass spectrometry (ICP-MS) is a powerful technique for trace multielement and isotopic analysis, because of its high sensitivity and ability to determine the isotope composition of sample.

However, ICP-MS is prone to interferences caused by sample matrix components. The interferences may be caused by polyatomic ions having the same nominal mass as the analyte, signal suppression or enhancement due to nonspectroscopic matrix effect and blockage of the nebulizer and sampler. Therefore, in order to achieve accurate and reliable results, matrix separation is needed when the matrix elements in the prepared solution interfere with the determination. [27] The fundamental parts of an ICP-MS are the following shown in the Figure 4.2.

An introduction system where the samples in liquid form are transported to a nebulizer system by usually a peristaltic pump. Then, it is transformed into a spray composed of light drops by means of an incident argon flow. Following, takes place the ionization, where plasma is generated on top of a torch. When nebulized sample enters in the plasma, it is instantaneously desolvated and atomized; then atoms are turned into ions depending on the potential of respective elements. Then, vapor that contains ions and atoms is driven by argon through an interface. Finally, the quadrupole allows the separations of ions and the electron multipliers transforms those ions signals into electric pulses.[27] [28]

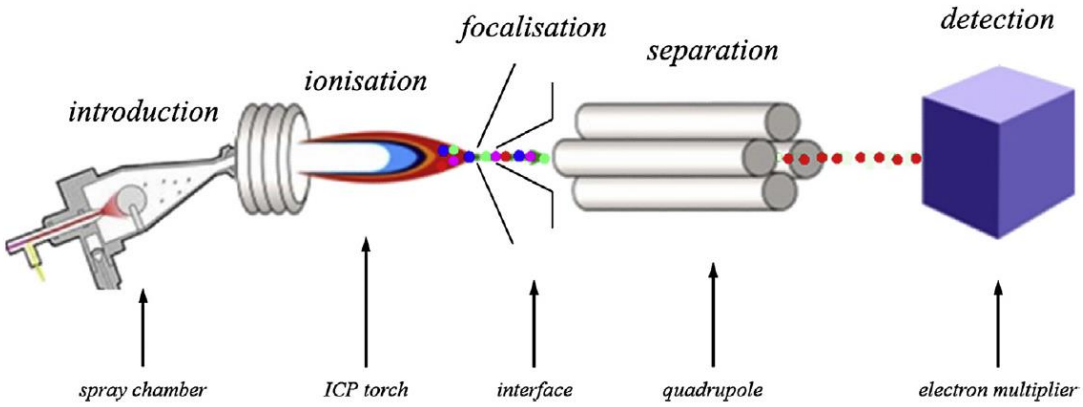

Figure 4.2. Scheme of an ICP-MS system. [28]

4.4 Brunauer- Emmett- Teller (BET)

The Brunauer- Emmett- Teller (BET) method is commonly applied to calculate the specific surface area of materials. This information is used to predict the dissolution rate, as the rate is proportional to the specific surface area (m^2/g). BET theory applies to systems of multilayer absorption and usually probing gases that do not chemically react with the material surfaces as adsorbates to quantify specific surface are. Nitrogen is the most commonly employed gaseous adsorbate used for probing by BET methods. [29]

5. Results and discussion

5.1 Characterization of Gd_2O_3-UO_2 pellets

5.1.1 SEM characterization

SEM technique allows to verify that the pellets present microstructures and to determine the composition of U and Gd.

Figure 5.1 was obtained with the SEM equipment, in which it can be observed a homogenous and non-porous microstructure obtained in the synthesis of gadolinium doped with UO_2. It was also determined the composition at a selected point within one of the grains, observing both uranium and gadolinium.

Comparing the results in Figure 5.1 and Figure 5.2, it is possible to observe how in the 10% wt. Gd-doped pellet the composition of Gd is double than in the 5% wt.

In both cases, various points were selected in order to compare the results and check that at any point the concentration is homogeneous.

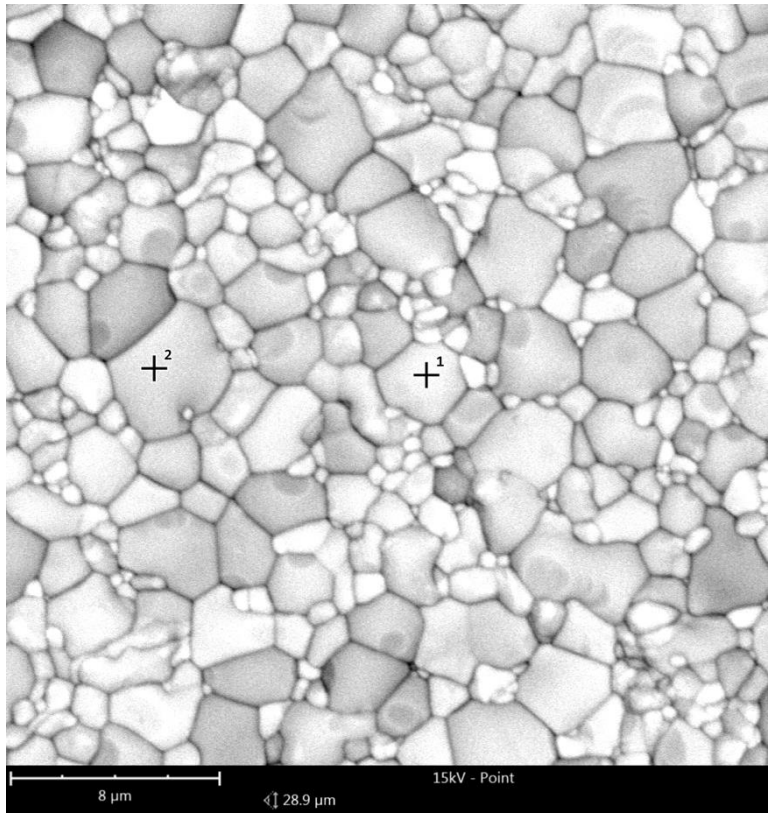

1

Weight percentage

U	85.25 %
C	5.11 %
O	4.72 %
Gd	3.13 %
N	1.79 %

2

Weight percentage

U	84.69 %
C	4.91 %
O	4.42 %
Gd	3.61 %
N	1.73 %
Ag	0.65 %

Figure 5.1. Left: Image obtained by SEM. Right: EDS study performed on the 5% wt. Gd-doped pellet.

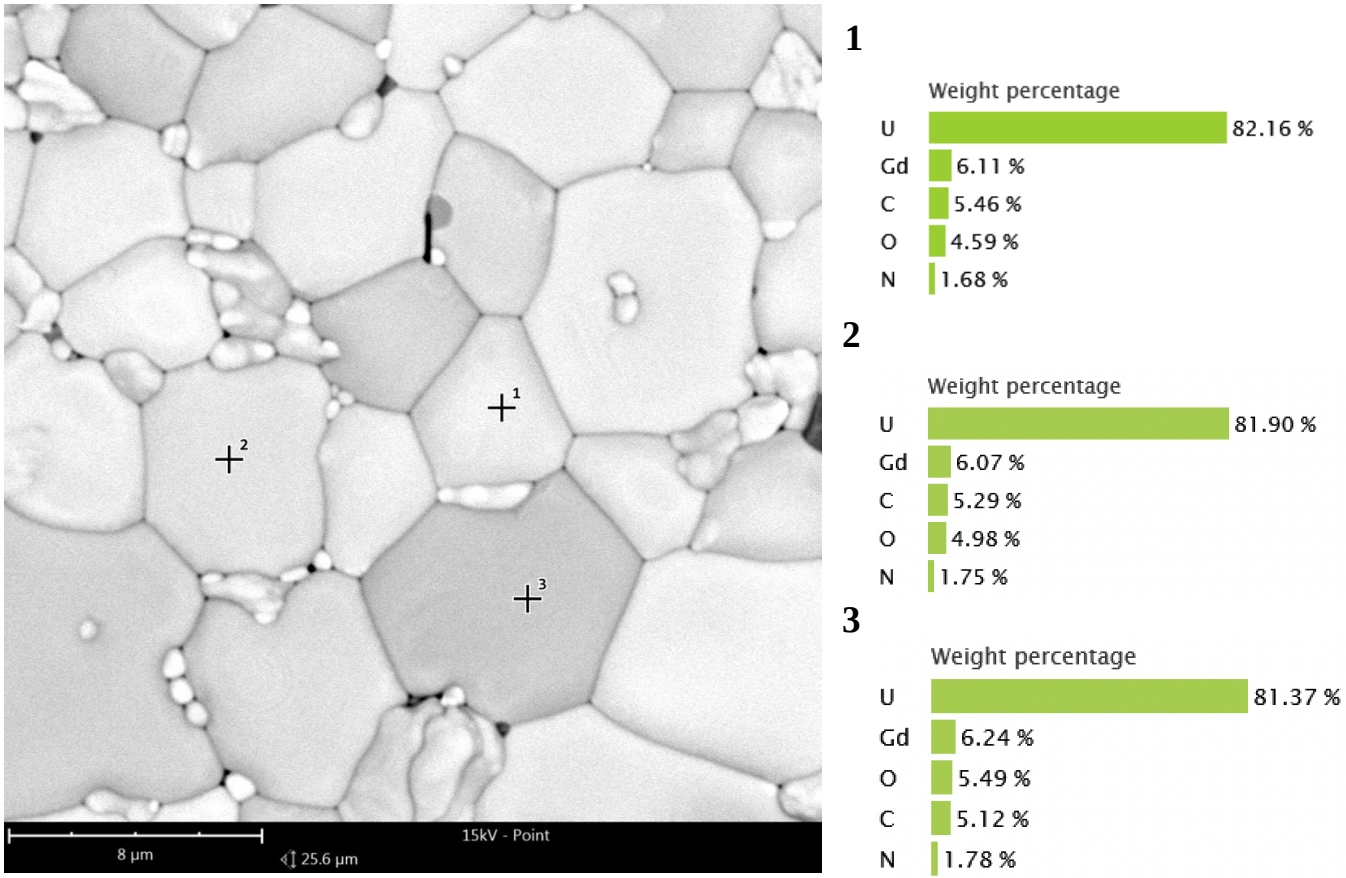

Figure 5.2. Left: Image obtained by SEM. Right: EDS study performed on the 5% wt. Gd-doped pellet.

5.1.2 X-ray characterization

In some studies, as Durazzo 2010 or the X-ray performed by Baena in 2015, a clear, systematic peak shift towards higher angles is observed corresponding to a lattice contraction with increasing gadolinium content (Figure 5.3).

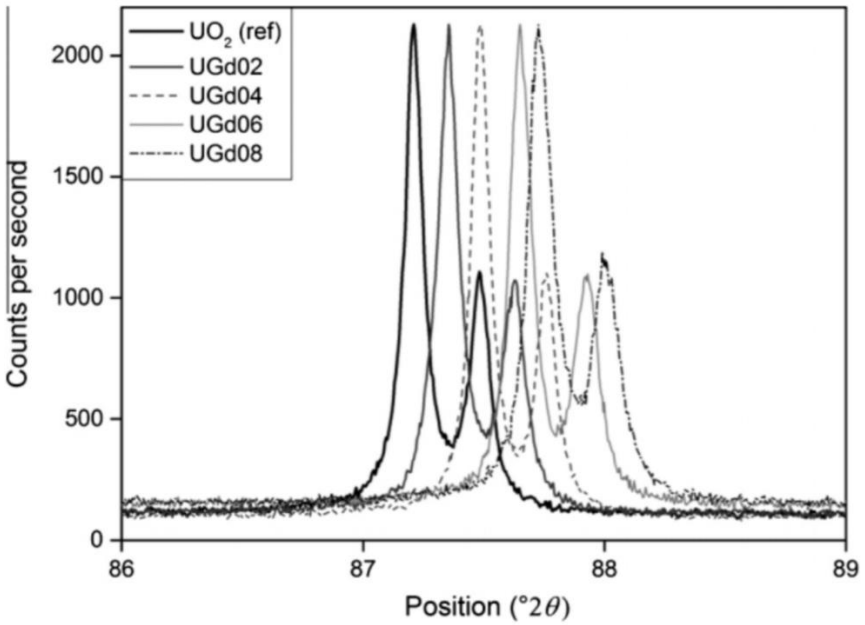

Figure 5.3. X-ray performed by Baena showing the displacement [16]

X-ray diffraction analysis in the Figure 5.4 showed the presence of only one crystalline phase (fluorite type) for all the samples represented, which indicates the Gd is homogeneously distributed within the UO_2 matrix, maintaining the same structure. It shows the peaks of the diffractograms of the two doped samples 5% Gd_2O_3 (in red) and 10% Gd_2O_3 (in grey) and the diffractogram of the pure UO_2 is added as a reference (in blue). [16]

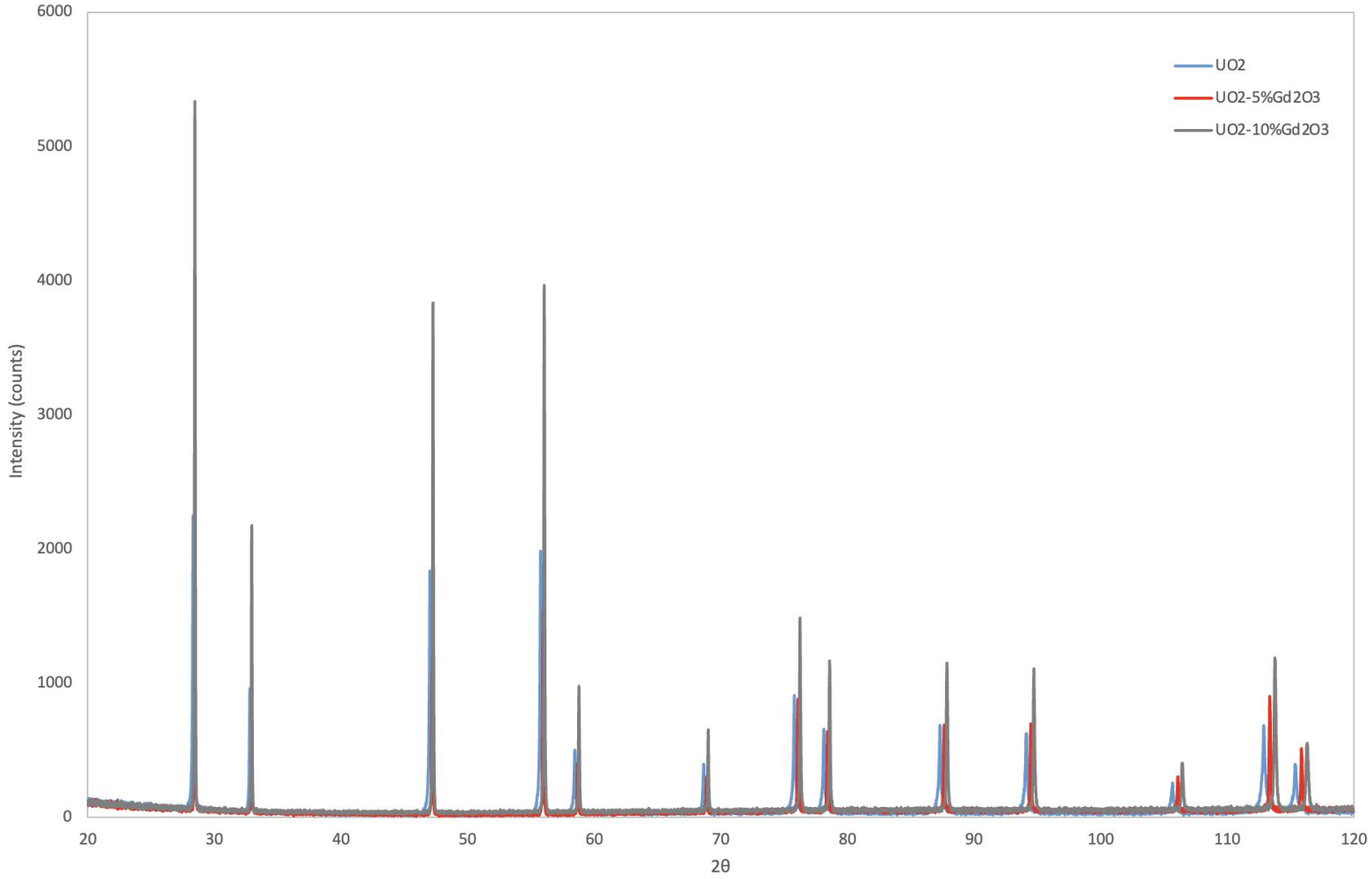

Figure 5.4. XDR spectrum and characteristics peaks for UO_2 and Gd_2O_3.

5.2 Kinetics of dissolution

In order to determine the flow rate to work on, a study of the concentration of dissolved U and Gd versus the inverse of the flow rate was done at constant pH. If a linearity was obtained, then these concentrations correspond to a steady state under these conditions and the kinetic of dissolution is therefore independent of the flow rate.

In this project, as three different reactors were assembled, it was performed a study for each reactor at a constant pH=3 at different flow rates. The results are shown in Table 5.1, Table 5.2 and Table 5.3.

Table 5.1. Study linearity Reactor A (pure UO_2)

pH	U Conc. [mol/L]	Gd Conc. [mol/L]	Q [mL/min]	1/Q [min/mL)
3,00	$1{,}26(\pm0{,}10)\cdot10^{-6}$	---	0,050	20,20
3,00	$8{,}46(\pm0{,}08)\cdot10^{-7}$	---	0,073	13,67
3,00	$6{,}34(\pm0{,}02)\cdot10^{-7}$	---	0,100	10
3,00	$4{,}80(\pm0{,}02)\cdot10^{-7}$	---	0,122	8,22

Table 5.2. Study linearity Reactor B (UO_2 doped with 5% Gd_2O_3)

pH	U Conc. [mol/L]	Gd Conc. [mol/L]	Q [mL/min]	1/Q [min/mL)
3,00	$7{,}87(\pm0{,}95)\cdot10^{-7}$	$6{,}48(\pm0{,}03)\cdot10^{-8}$	0,050	20,20
3,00	$5{,}30(\pm0{,}01)\cdot10^{-7}$	$4{,}73(\pm0{,}04)\cdot10^{-8}$	0,073	13,67
3,00	$4{,}36(\pm0{,}01)\cdot10^{-7}$	$3{,}67(\pm0{,}06)\cdot10^{-8}$	0,099	10,10
3,00	$3{,}3(\pm0{,}01)\cdot10^{-7}$	$2{,}79(\pm0{,}04)\cdot10^{-8}$	0,122	8,22

Table 5.3. Study linearity Reactor C (UO_2 doped with 10% Gd_2O_3)

pH	U Conc. [mol/L]	Gd Conc. [mol/L]	Q [mL/min]	1/Q [min/mL)
3,00	$9{,}71(\pm0{,}67)\cdot10^{-7}$	$9{,}71(\pm2{,}10)\cdot10^{-7}$	0,050	20,20
3,00	$6{,}19(\pm0{,}30)\cdot10^{-7}$	$6{,}19(\pm1{,}27)\cdot10^{-7}$	0,073	13,67
3,00	$5{,}10(\pm0{,}60)\cdot10^{-7}$	$5{,}11(\pm1{,}42)\cdot10^{-7}$	0,099	10,10
3,00	$3{,}56(\pm0{,}35)\cdot10^{-7}$	$3{,}56(\pm0{,}07)\cdot10^{-7}$	0,122	8,22

Then, with the data obtained in the laboratory and calculated later, it is represented the two graphs for both uranium and gadolinium concentrations versus the inverse of flow rate. The results can be seen in Figure 5.5 and Figure 5.6. Thus, concentrations are represented in mol/L and the inverse of the flow rate is represented in min/mL.

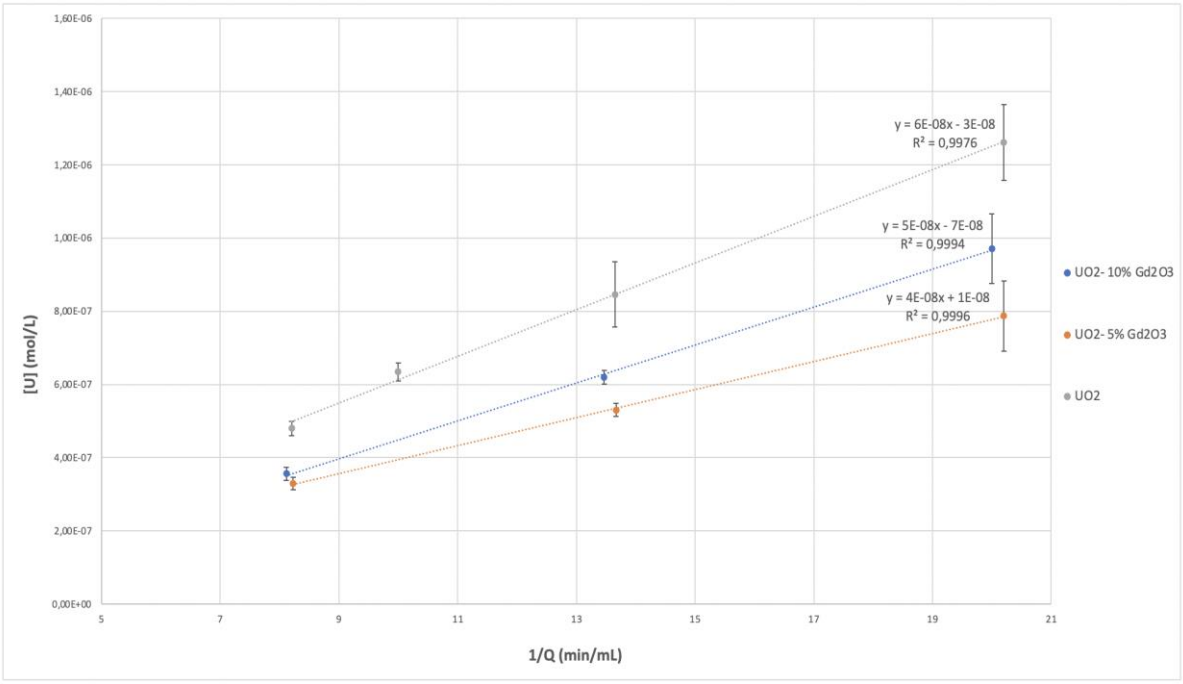

Figure 5.5. Variation of U concentration as a function of the inverse of the flow rate.

In Figure 5.5 and Figure 5.6, the U concentration and Gd concentration, respectively, are represented as a function of the inverse of the flow rate. The results present a linearity in the studied range (0,050-0,12 mL/min).

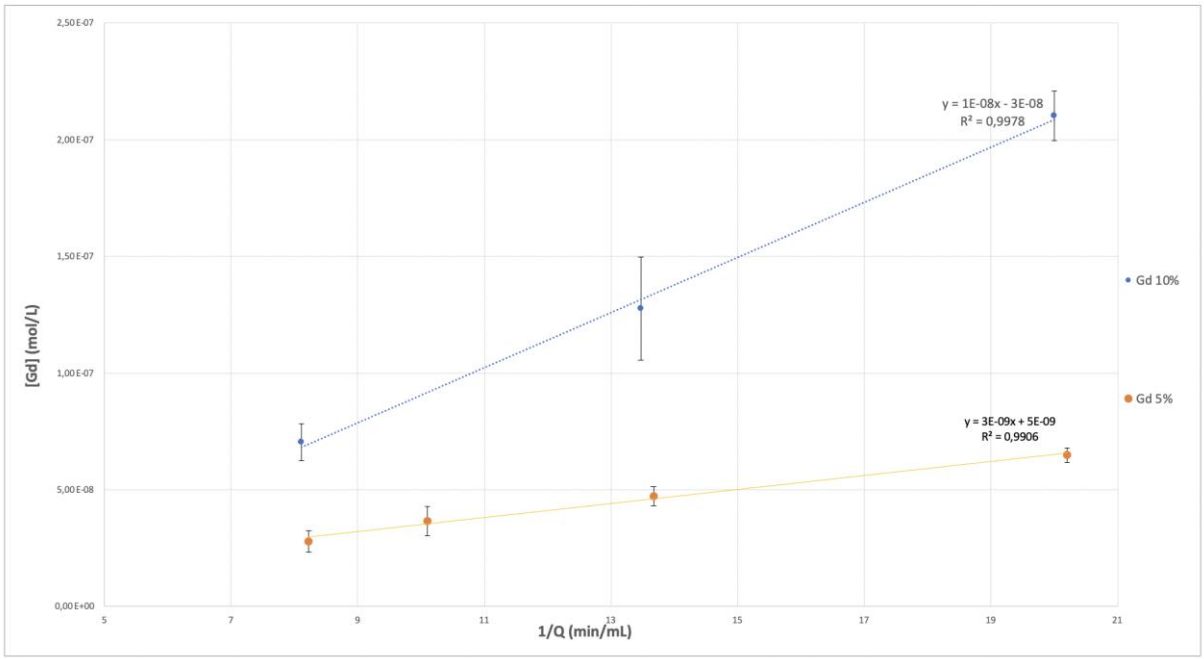

Figure 5.6. Variation of Gd concentration as a function of the inverse of the flow rate.

Once the study confirms that under these conditions the system is in steady state, it will be possible to study the kinetics of dissolution in this flow range. Therefore, a flow rate under this range can be fixed constant.

The next experiments were performed under a wide range of pH from 2 to 13 at 0.8 mL/min. In order to observe the presence of reactive phases from the bulk uranium dioxide, samples were collected since the first moment.

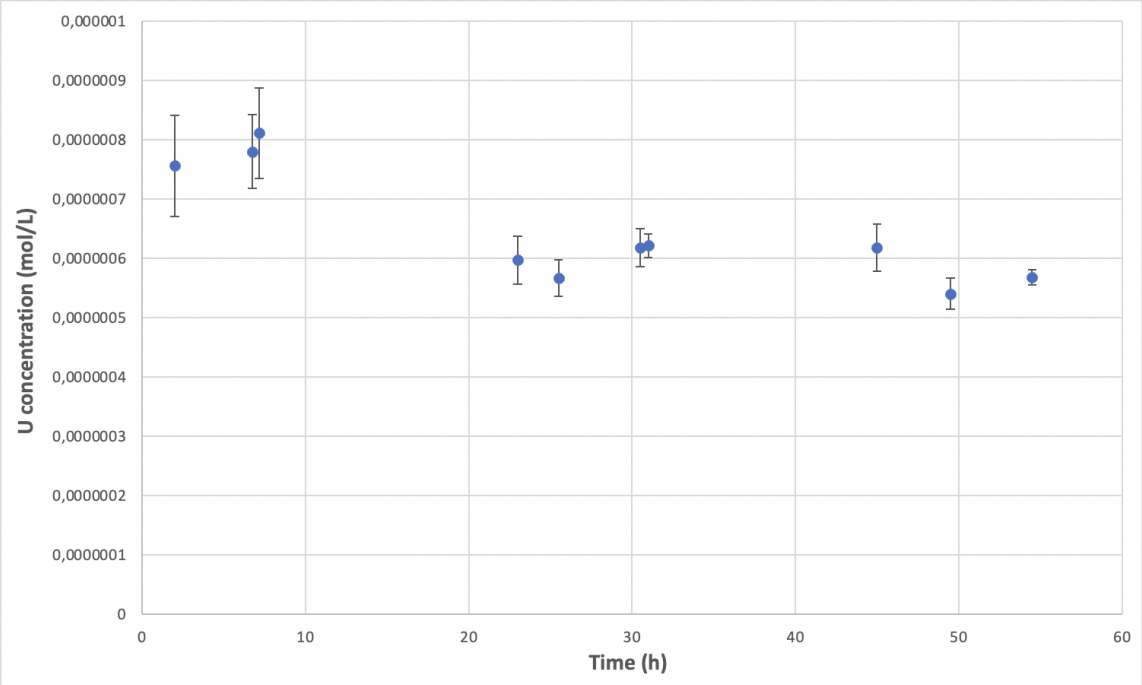

Figure 5.7. Uranium concentration obtained at pH 10 since the settled up of the system.

As shown in Figure 5.7, after the first 24 hours, the concentration starts to stabilize, reaching a steady state. Therefore, this situation is similar to the one proposed in Figure 3.4, in the study carried out by Bruno in 1990.

Once the system has been started up, samples were collected and taken to ICP-MS to calculate the uranium and gadolinium concentrations. Then, results were analyzed and an average is obtained for each pH studied. Using the equations (7)-(8) and (9)-(10) dissolution rate values and normalized dissolution rates (NDR) values were calculated and plotted (Figure 5.8 and Figure 5.10).

5.2.1 Kinetics of dissolution of uranium

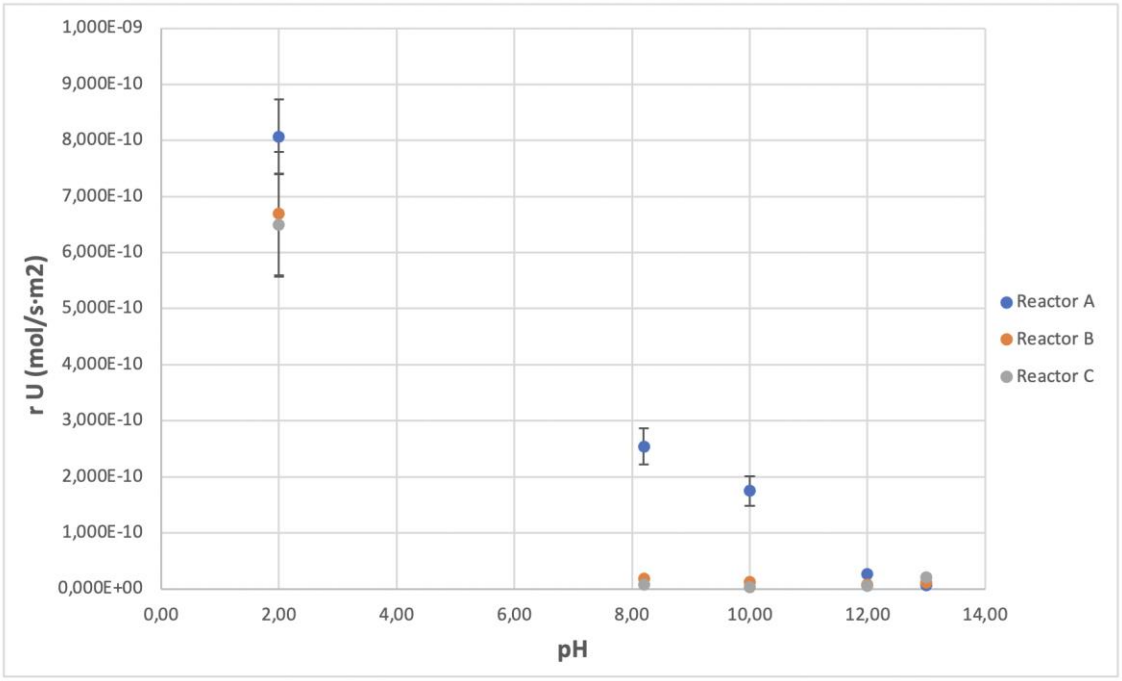

Figure 5.8. Uranium dissolution rate in the pH studied.

In Figure 5.8, it is observed the effect of gadolinia (reactor B and C) especially at pH 8 and 10, where the dissolution of the uranium is inhibited in Reactor B (UO_2-5%Gd_2O_3) and C (UO_2-5%Gd_2O_3), compared to reactor A (UO_2). Also, dissolution rate values of UO_2 at hyperalkaline conditions are very low for the three samples. That is an interesting point, since lowering dissolution rate of UO_2 under alkaline and hyperalkaline conditions is a great advantage for a deep geological repository from the point of view of safety.

In figure 5.9 the logarithm of the normalized dissolution rate of U was represented versus the pH range studied. In this plot the effect of gadolinium in alkaline pH (pH 8 and 10) is clearly evident. However, in acidic pH the effect of gadolinia is less significant.

This behaviour is similar to the study proposed by Casella et al. [23], in which the addition of gadolinia into the UO_2 matrix resulted in a significant decrease in the dissolution rate of UO_2 at different temperatures, even where the rates would typically be elevated.

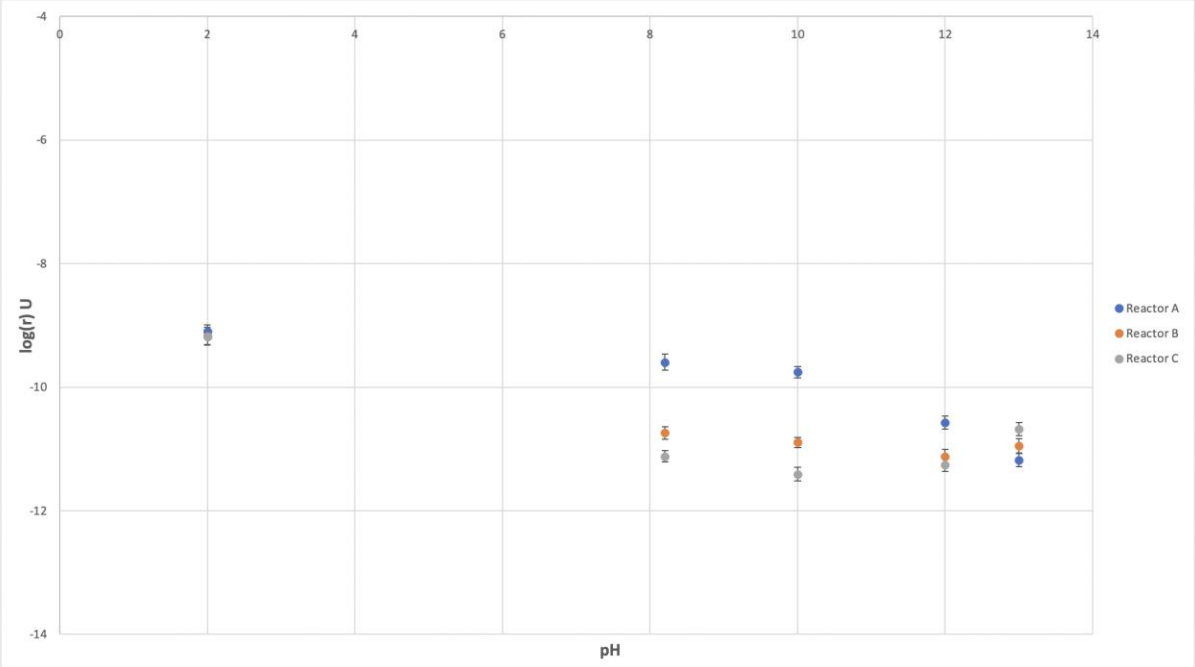

Figure 5.9. Logarithm of uranium dissolution rate of UO_2 in the pH range studied.

In reactor A, two behaviors are distinguished, from pH 2 to 10 and from 10 to 13. Thus, two different equations can be obtained from Figure 5.10.

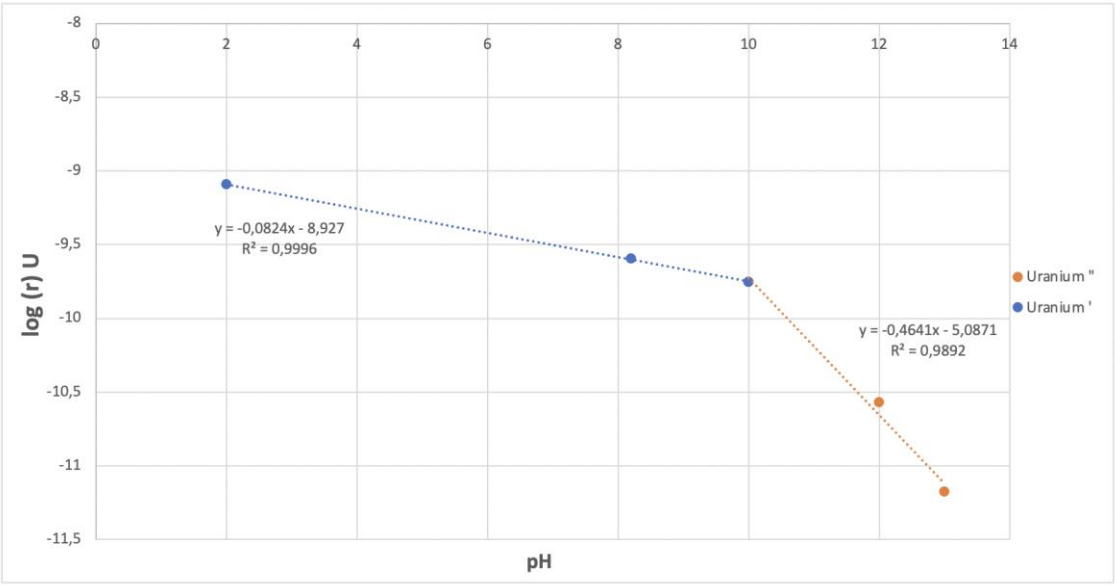

Figure 5.10. Behavior of uranium's dissolution rate logarithm in Reactor A.

In the first range of pH, from 2 to 10, it is observed a not very pronounced behavior described by the next equation:

$$\log (r) = -0{,}08(\pm 0.01) \cdot (-\log([H^+])) - 8{,}93(\pm 0{,}01) \qquad (14)$$

The quadratic correlation coefficient is $R^2 = 0{,}9996$, in which isolating the equation (14) is obtained:

$$\log (r) = \log [H^+]^{0{,}08(\pm 0{,}01)} - 8{,}93(\pm 0{,}01)$$

$$\mathbf{r\ (mol/\ s^{-1} \cdot m^{-2}) = 10^{-\ 8{,}93(\pm 0{,}01)} \cdot [H^+]^{0{,}08(\pm 0{,}01)}} \qquad \mathbf{(15)}$$

In the second range, from 10 to 13, the decrease of the uranium dissolution rate is more pronounced. The behavior is explained by the next equation:

$$\log (r) = -0{,}46(\pm 0.05) \cdot (-\log([H^+])) - 5{,}09(\pm 0{,}57) \qquad (16)$$

The quadratic correlation coefficient is $R^2 = 0{,}9892$. Then, isolating the equation (16) is obtained:

$$\log (r) = \log [H^+]^{\,0{,}46(\pm 0{,}05)} - 5{,}09(\pm 0{,}57)$$

$$\mathbf{r\ (mol/\ s^{-1} \cdot m^{-2}) = 10^{-5{,}09\ (\pm 0{,}57)} \cdot [H^+]^{\,0{,}46(\pm 0{,}05)}} \qquad \mathbf{(17)}$$

Same procedure is followed in the Reactor B and C, where the kinetics of dissolution of the uranium are studied. In this case, the pH ranges are from 2 to 10, since no tendency was observed from 10 to 13.

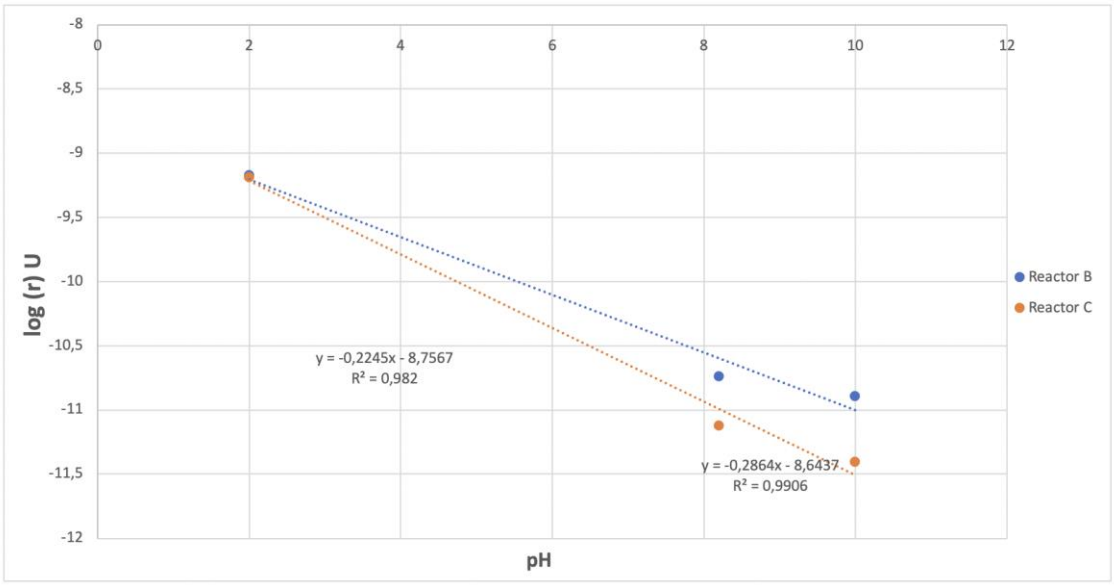

Figure 5.11. Behavior of uranium's dissolution rate logarithm in Reactor B and C.

In this range of pH, the behavior for the Reactor B is described by the next equation:

$$\log (r) = -0{,}22(\pm 0{,}03) \cdot (-\log([H^+])) - 8{,}76(\pm 0{,}23) \quad (18)$$

The quadratic correlation coefficient is $R^2 = 0{,}982$. Thus, isolating the equation (18) it is obtained:

$$\log (r) = \log [H^+]^{0{,}22(\pm 0.03)} - 8{,}76(\pm 0{,}23)$$

$$\mathbf{r\ (mol/\ s^{-1} \cdot m^{-2}) = 10^{-\,8{,}76(\pm 0{,}23)} \cdot [H^+]^{0{,}22(\pm 0{,}03)}} \quad \mathbf{(19)}$$

In Reactor C same tendency is presented, which is described by the next equation:

$$\log (r) = -0{,}29(\pm 0{,}03) \cdot (-\log([H^+])) - 8{,}64(\pm 0{,}21) \quad (20)$$

The quadratic correlation coefficient is $R^2 = 0{,}9906$. Isolating the equation (20) is obtained:

$$\log (r) = \log [H^+]^{0{,}29(\pm 0.03)} - 8{,}64(\pm 0{,}21)$$

$$\mathbf{r\ (mol/\ s^{-1} \cdot m^{-2}) = 10^{-\,8{,}64(\pm 0{,}21)} \cdot [H^+]^{0{,}29(\pm 0{,}03)}} \quad \mathbf{(21)}$$

The slope of the lines in Figure 5.11 is slightly higher for Reactor C than Reactor B. This behaviour could be due to the higher amount of %Gd in C than in B, and therefore its influence in uranium dissolution decrease could be higher.

Although the equations, (15), (17), (19) and (21) represent different pH ranges, in all cases the protons dependency is a positive value, which means the dissolution mechanism is produced by superficial complexation, specifically, is produced by a superficial protonation.[30]

5.2.2 Kinetics of dissolution of gadolinium

Figure 5.12 shows the dissolution rate of gadolinium in reactors B and C. It can be seen that at acidic pH the dissolution rate of gadolinium is high, whereas in alkaline pH it decreases, reaching the lowest rates at hyperalkaline conditions (pH higher than 12).

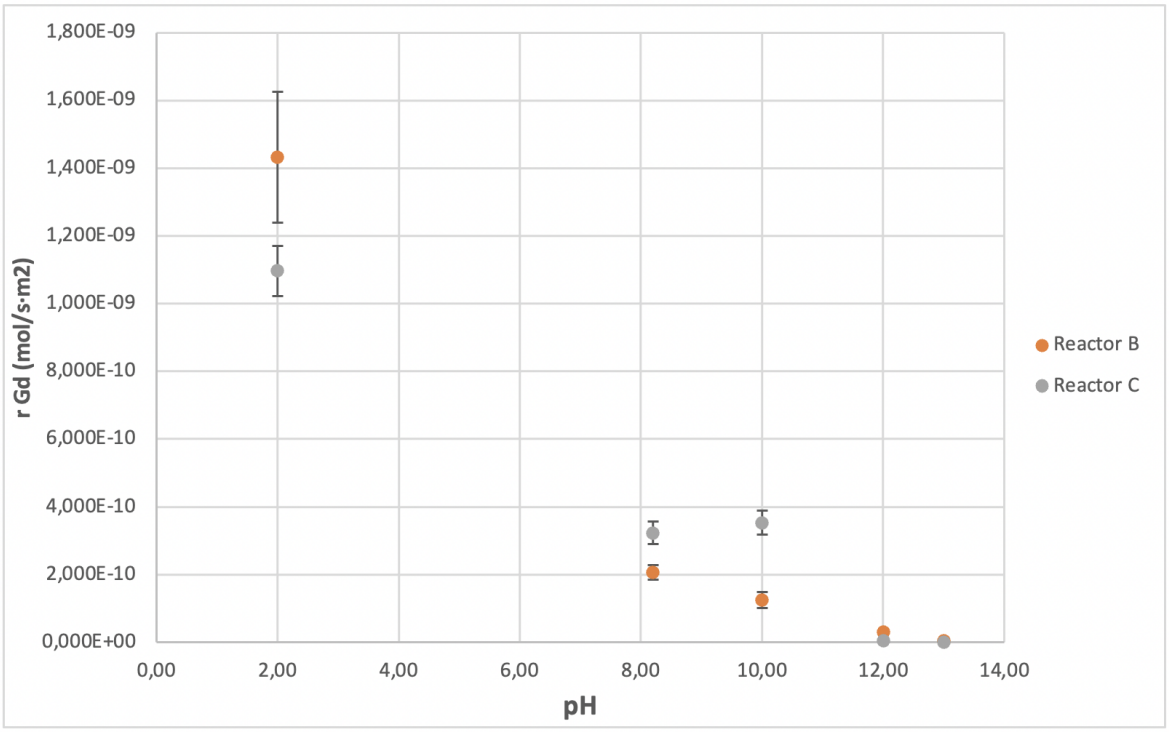

Figure 5.12. Gadolinium dissolution rate in the pH studied.

In Figure 5.13, the values of logarithm of Gd dissolution rate shows that at higher pH, the dissolution rate decay is very pronounced and gadolinium barely dissolves.

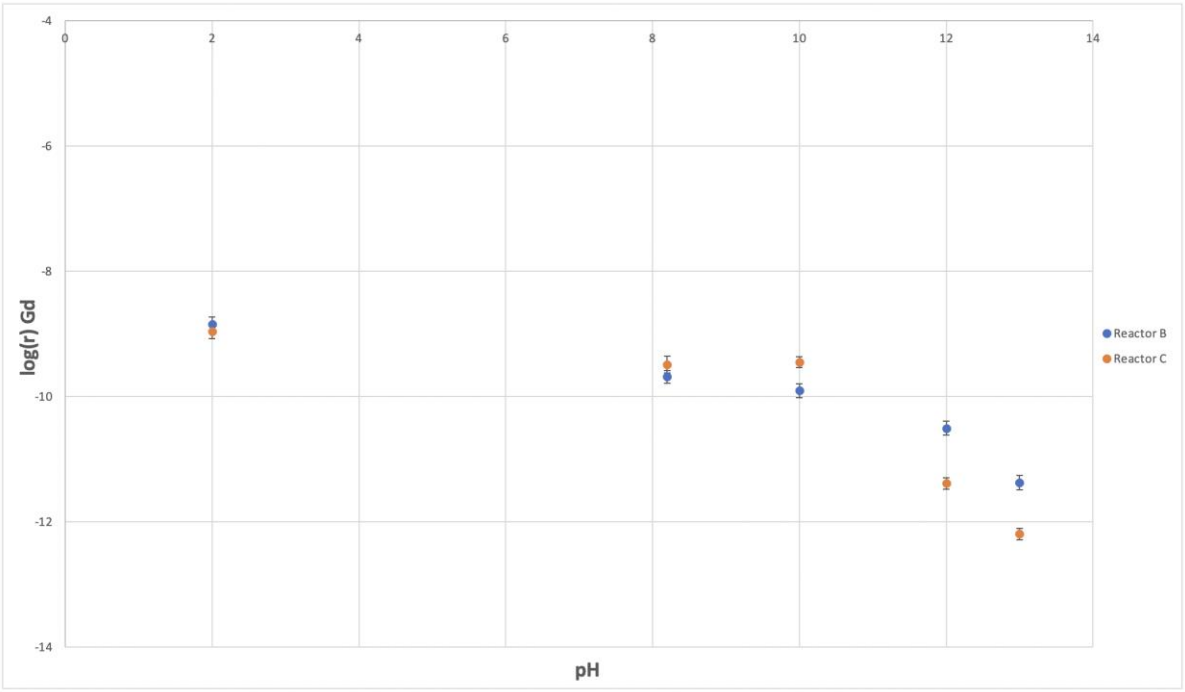

Figure 5.13. Logarithm of gadolinium dissolution rate in the pH range studied.

Regarding to gadolinium's behavior in reactor B, two tendencies are distinguished, from pH 2 to 10 and from 10 to 13. Then, two different equations can be obtained from the Figure 5.14.

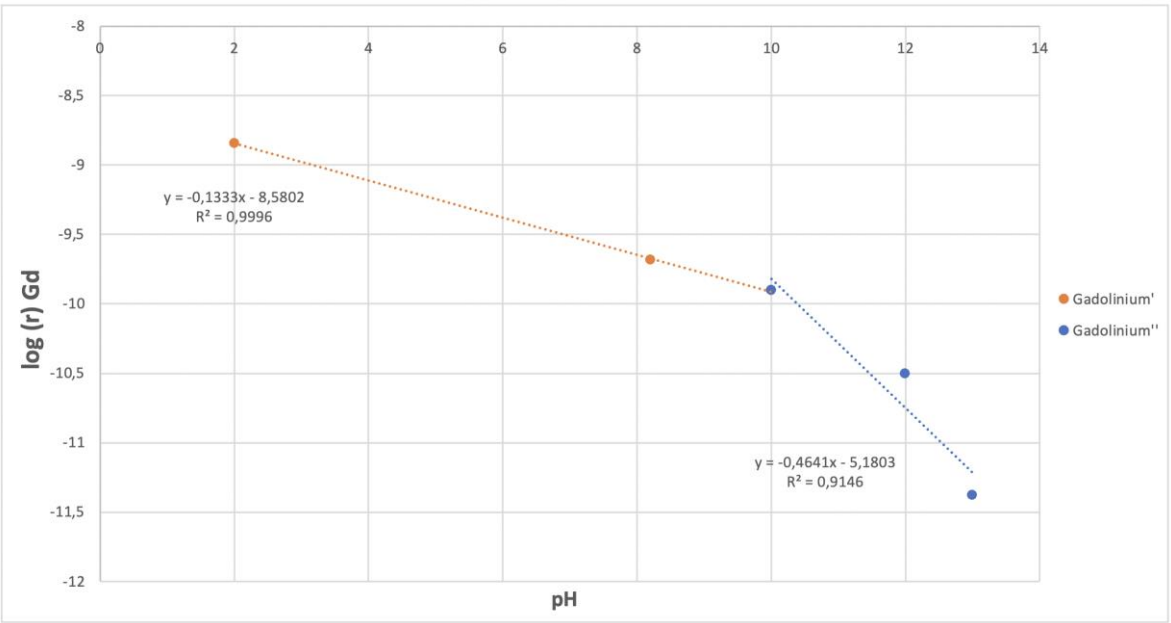

Figure 5.14. Behavior of the gadolinium's dissolution rate logarithm in Reactor B.

The first range, from 2 to 10, its behavior is explained by the next equation:

$$\log (r) = -0{,}13(\pm 0{,}01) \cdot (-\log([H^+])) - 8{,}58(\pm 0{,}02) \qquad (22)$$

The quadratic correlation coefficient is $R^2 = 0{,}9996$. Finally, it is obtained:

$$\log (r) = \log [H^+]^{0{,}13(\pm 0{,}01)} - 8{,}58(\pm 0{,}02)$$

$$\mathbf{r\ (mol/\ s^{-1} \cdot m^{-2}) = 10^{-\ 8{,}58(\pm 0{,}02)} \cdot [H^+]^{0{,}13(\pm 0{,}01)}} \qquad \mathbf{(23)}$$

In the second range, from 10 to 13, the decrease of the gadolinium dissolution rate is more pronounced. The behavior is described by the next equation:

$$\log (r) = -0{,}46(\pm 0{,}14) \cdot (-\log([H^+])) - 5{,}18(\pm 1{,}66) \qquad (24)$$

The quadratic correlation coefficient is $R^2 = 0{,}9142$ and isolating the (23) is obtained:

$$\log (r) = \log [H^+]^{\ 0{,}46(\pm 0{,}14)} - 5{,}18(\pm 1{,}66)$$

$$\mathbf{r\ (mol/\ s^{-1} \cdot m^{-2}) = 10^{-5{,}18\ (\pm 1{,}66)} \cdot [H^+]^{\ 0{,}46(\pm 0{,}14)}} \qquad \mathbf{(25)}$$

Same procedure is followed in the Reactor C, where the kinetics of dissolution of the gadolinium were studied.

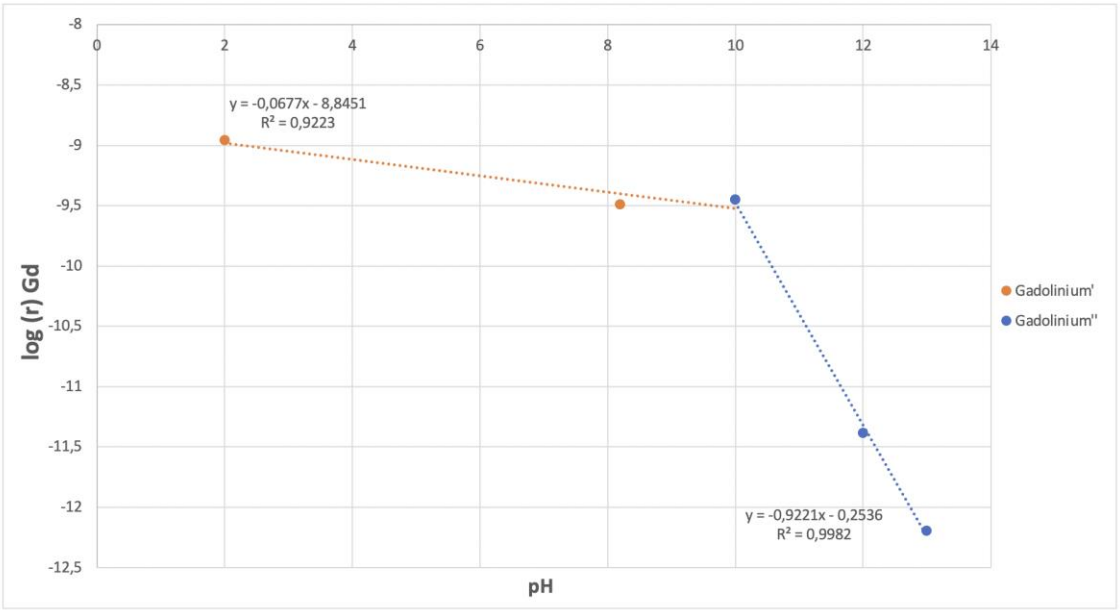

Figure 5.15. Behavior of the gadolinium's dissolution rate logarithm in Reactor C.

In the first range, it is observed a less pronounced decrease behavior than in Figure 5.14 and is described by the next equation for the Reactor C:

$$\log (r) = -0{,}07(\pm 0{,}02) \cdot (-\log([H^+])) - 8{,}85(\pm 0{,}15) \qquad (26)$$

The quadratic correlation coefficient is $R^2 = 0{,}9223$. Finally, isolating the previous equation is obtained:

$$\log (r) = \log [H^+]^{0{,}07(\pm 0{,}02)} - 8{,}85(\pm 0{,}15)$$

$$\mathbf{r\ (mol/\ s^{-1} \cdot m^{-2}) = 10^{-\ 8{,}85(\pm 0{,}15)} \cdot [H^+]^{0{,}07(\pm 0{,}02)}} \qquad \mathbf{(27)}$$

In the second range, from 10 to 13, there is a more pronounced decrease in the dissolution rate of gadolinium (Figure 5.15). The behavior is explained by the next equation:

$$\log (r) = -0{,}92(\pm 0{,}04) \cdot (-\log([H^+])) - 0{,}25(\pm 0{,}46) \qquad (27)$$

The quadratic correlation coefficient is $R^2 = 0{,}9982$ and isolating the equation (28) it is obtained:

$$\log (r) = \log [H^+]^{0,92(\pm 0,04)} - 0,25(\pm 0,46)$$

$$\mathbf{r\ (mol/\ s^{-1} \cdot m^{-2}) = 10^{-0,25\ (\pm 0,46)} \cdot [H^+]^{0,92(\pm 0,04)}} \qquad \mathbf{(29)}$$

As uranium behaviour, the dissolution mechanism of gadolinium is also produced by superficial complexation, specifically, is produced by a superficial protonation.[30]

Finally, a summary is presented with all the different equations for a pH range from 2 to 10 and for each reactor.

Table 5.4. Equations in Reactor A for a pH from 2 to 10

Reactor A	Equation
Uranium	$r\ (mol/\ s^{-1} \cdot m^{-2}) = 10^{-8,93(\pm 0,01)} \cdot [H^+]^{0,08(\pm 0.01)}$

Table 5.5. Equations in Reactor B for a pH from 2 to 10

Reactor B	Equation
Uranium	$r\ (mol/\ s^{-1} \cdot m^{-2}) = 10^{-8,76(\pm 0,23)} \cdot [H^+]^{0,22(\pm 0,03)}$
Gadolinium	$r\ (mol/\ s^{-1} \cdot m^{-2}) = 10^{-8,58(\pm 0,02)} \cdot [H^+]^{0,13(\pm 0,01)}$

Table 5.6. Equations in Reactor C for a pH from 2 to 10

Reactor C	Equation
Uranium	$r\ (mol/\ s^{-1} \cdot m^{-2}) = 10^{-8,64(\pm 0,21)} \cdot [H^+]^{0,29(\pm 0,03)}$
Gadolinium	$r\ (mol/\ s^{-1} \cdot m^{-2}) = 10^{-8,85(\pm 0,15)} \cdot [H^+]^{0,07(\pm 0,02)}$

In Figure 5.16 and Figure 5.17 it can be seen that kinetics of dissolution of gadolinium is higher than the uranium's. Therefore, it does not dissolve congruently, since the kinetics of dissolution of gadolinium does not match with the kinetics of dissolution of uranium under the pH range from 2 to 10.

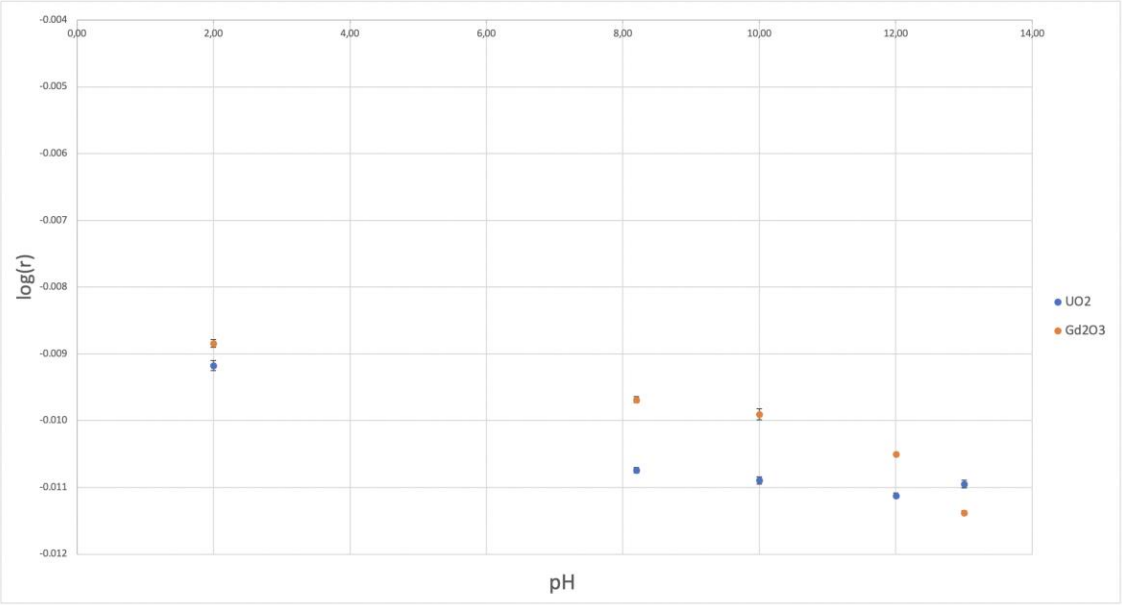

Figure 5.16. Comparative between dissolution rate logarithm of gadolinium and uranium in Reactor B.

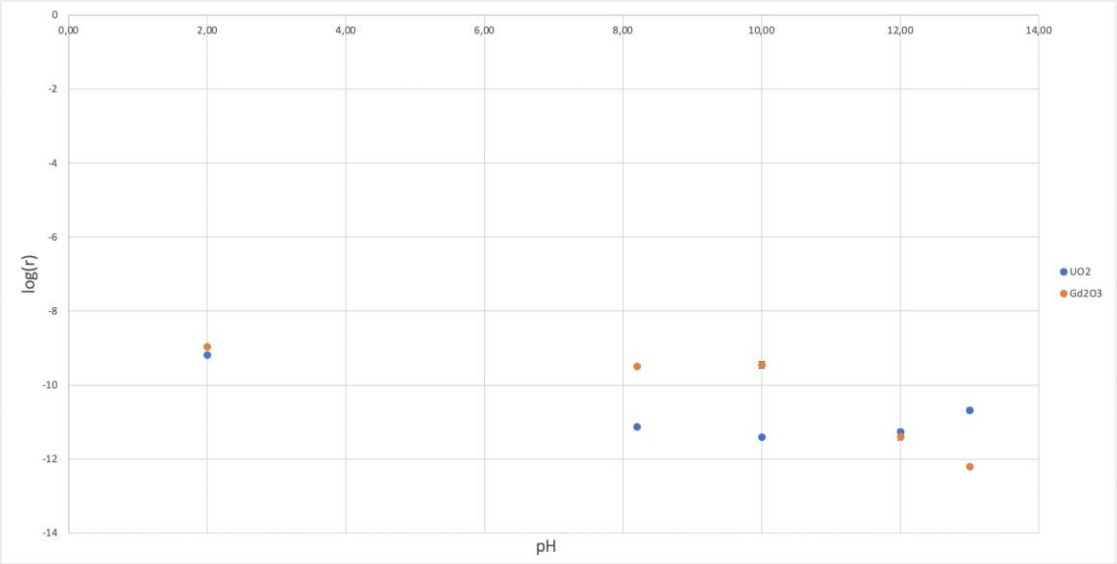

Figure 5.17. Comparative between dissolution rate logarithm of gadolinium and uranium in Reactor C.

6 Conclusions

It is considered that this project has achieved the proposed objectives, obtaining the following conclusions:

Regarding the synthesis and characterization with SEM and XRD of the UO_2 doped with Gd_2O_3:

- UO_2-Gd doped pellets have been well sintered in the furnace at 1740ºC under reducing conditions.
- It has been observed with SEM that the pellets presented a homogeneous composition and non-porous microstructure. In addition, the observed compositions corresponded to the theoretical compositions of each pellet.
- XRD showed the presence of only one crystalline phase (fluorite type) for the samples represented.

Regarding the kinetics of dissolution of uranium and gadolinium:

- A continuous thin-film reactor has been started-up and the kinetics of dissolution of the uranium and gadolinium have been studied.
- A flow range to work in the steady state conditions has been established.
- The influence of gadolinium and pH on the UO_2 dissolution rate has been evaluated and determined.
- It has been proved that the addition of gadolinia resulted in a significant decrease in the dissolution rate of uranium oxide.
- It has been showed that in groundwater conditions (alkaline and hyper alkaline pH) the uranium dissolution rate is the lowest for all the pH range studied.

7 Waste management

Regarding the waste treatment, it depends on whether it is an adsorbent solid or a solution that contains uranium.

Solids that have been in contact with uranium, such as gloves, papers or filters will be stored in a plastic bag and once filled they are weighted and its emitted radiation is measured.

The "Consejo de Seguridad Nacional" of Spain, established in 2010 that emitted radiation in solids that exceed 50 mSv, will be classified as radioactive and requires a complex process and treatment. But, if the emitted radiation is lower than 50 mSV, the concentration will be classified as negligible and will be treated as a normal waste.

When a solution contains uranium that comes from the reactor or a cleaning process, it is stored in a waste bottle, as shown in Figure 3.5. This bottle is classified as a containing heavy metals aqueous acid inorganic solution, in which samples are taken. The liquid residues are treated by "FCC Ámbito".

Thus, the used material that may contain UO_2 powder is also cleaned with nitric acid 2% in weight, that oxides from U(IV) to U(VI), facilitating the cleaning process because U(VI) is more soluble in water.

8 Economic study

The estimated expenses of this project are detailed in this section. It is structured in costs of equipment, costs of laboratory supply and reagents, analytical costs and human resources costs:

The equipment costs are calculated as an amortization cost in function of the time that have been used in the project and its useful lifetime. Also, it is considered that the amortization cost does not vary over the time.

Finally, the total gross cost, taxes and the final net cost of the project will be shown, as well as the Figure 7.1, in which percentages of each cost will be represented.

$$Amortization\ cost\ (€) = \frac{Acquisition\ cost}{useful\ lifetime} \cdot using\ time$$

Table 7.1. Calculation of the amortization costs of the equipment

Equipment	Acquisition cost [€]	Useful lifetime [yr]	Using time [yr]	Amortization [€]
Peristaltic pump	1609,20	10	0,5	80,46
Manual press	2860,00	15	0,5	95,33
Horizontal tube furnace	22000,00	10	0,5	1100,00
Analytical balance	950,00	10	0,5	47,50
SUBTOTAL	-	-	-	**1323,29**

Table 7.2. Costs of reagents and laboratory supply.

Equipment	Price per unit [€]	Unit	Number	Cost [€]
Sodium Hydroxide 1M	33,90	1L	1	33,90
Nitric acid 90%	39,50	1L	0,1	3,95
Hydrochloric acid (37%)	21,10	1L	0,1	2,11
Sodium Hydrogen Carbonate	48,00	1Kg	0,01	0,48
Sodium perchlorate hydrogenated	314,00	1kg	0,25	78,50
Gadolinium (III) oxide	9,17	1 gr	0,3 gr	2,75
Millipore Milli-Q system	0,55	1L	20	11,00
Nitrogen Bottle	61,24	u	1	61,24
Argon 5% vol. hydrogen Bottle	87,33	u	1	87,33
Plastic test tubes 10 mL	0,12	u	360	43,20
Plug for plastic test tubes 10 mL	0,06	u	360	21,60
1mL pipette tips	0,06	u	100	6,00
5mL pipette tips	0,12	u	100	12,00
Nitrile gloves free powder	0,05	u	100	5,00
Millipore filters (diameter: 13 mm)	2,00	u	20	40,00
Other materials (flasks, pipettes…)	300	u	1	300,00
SUBTOTAL	-	-	-	**704,06**

Table 7.3. Analytical costs

Equipment	Quantity (samples/hours)	Price per quantity	Cost [€]
SEM-EDX	3 hours	48	144,00
XDR	3 samples	51,25	153,75
ICP-MS	360 samples	13	4680,00
BET	1 sample	110	110,00
SUBTOTAL	-	-	**5087,75**

Table 7.4. Human resources costs

Equipment	Price per hour [€]	Hours [h]	Cost [€]
Experimentation: Laboratory work	12	200	2400,00
Elaboration of the report	12	220	2640,00
SUBTOTAL	-	-	**5040,00**

Table 7.5. Total costs

			Cost [€]
Energy	0,1395 €/ KWh	200	27,90
Gross total cost	-	-	**12183,00**
V.A.T (21%)	-	-	**2558,43**
TOTAL COST	-	-	**14741,43**

Finally, a summary of the percentages of each cost are represented in Figure 7.1.

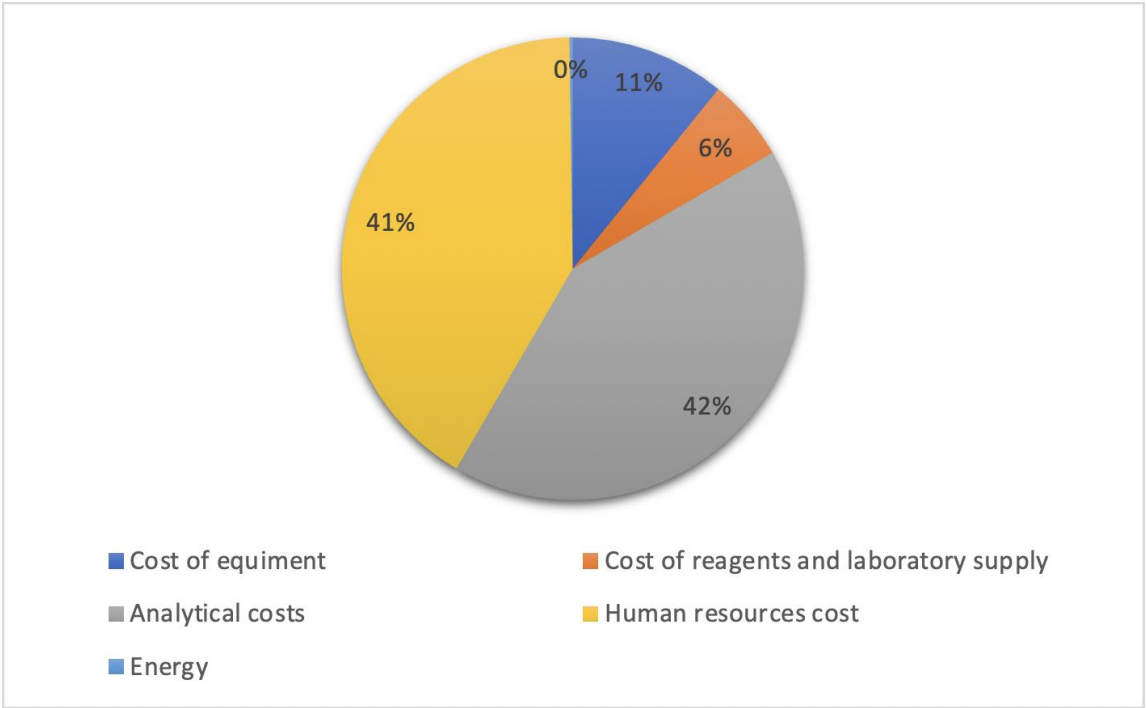

Figure 7.1. Percentages of the cost structures

9 Bibliography

[1] "NUCLEAR TECHNOLOGY," *Int. At. Energy Agency*, p. 77, 2020.

[2] "Borrador de 7º PGRR 16," pp. 1–114, 2020.

[3] R. C. Ewing, "Long-term storage of spent nuclear fuel," *Nat. Publ. Gr.*, vol. 14, no. 3, pp. 252–257, 2015, doi: 10.1038/nmat4226.

[4] "Radioactive waste management," *Inst. Radioprot. Sûreté Nuclêaire*, p. 28.

[5] J. A. Pastor, "Almacenamiento geológico profundo de residuos radiactivos de alta actividad (agp)," p. 204, 2001.

[6] Nuclear Waste Management Organization, *Deep Geological Repository Conceptual Design Report Crystalline / Sedimentary Rock Environment*, no. May. 2016.

[7] E. Environ, D. Cui, and K. Spahiu, "Environmental Science Environmental behaviors of spent nuclear fuel and canister materials," pp. 2537–2545, 2011, doi: 10.1039/c0ee00582g.

[8] D. P. L. Castro and K. M. V. Coral, "Caracterización y activación química de arcilla tipo bentonita para su evaluación en la efectividad de fenoles presentes en aguas residuales," p. 115, 2013.

[9] M. Gascoyne, *Influence of grout and cement on groundwater composition*, no. February. 2002.

[10] L. Duro, S. El, M. Rovira, J. De Pablo, and J. Bruno, "Study of the interaction between U (VI) and the anoxic corrosion products of carbon steel," vol. 23, pp. 1094–1100, 2008, doi: 10.1016/j.apgeochem.2008.01.004.

[11] D. W. Shoesmith, "The influence of dissolved hydrogen on the surface composition of doped uranium dioxide under aqueous corrosion conditions," vol. 602, pp. 8–16, 2007, doi: 10.1016/j.jelechem.2006.11.021.

[12] J. Bruno and R. C. Ewing, "Spent Nuclear Fuel," 2006.

[13] H. Kleykamp, "The chemical state of the fission' products in oxide fuels," vol. 131, pp. 221–246, 1985.

[14] D. W. Shoesmith, "Fuel corrosion processes under waste disposal conditions," vol. 282, pp. 1–31, 2000.

[15] T. Kubo and S. Ishimoto, "Effects of Gadolinium of UO2 Doping Grain on Electrical Properties Boundaries," vol. 672, pp. 664–672, 1993.

[16] A. Baena, T. Cardinaels, B. Vos, K. Binnemans, and M. Verwerft, "Synthesis of UO 2 and ThO 2 doped with Gd 2 O 3," vol. 461, pp. 271–281, 2015, doi: 10.1016/j.jnucmat.2015.03.028.

[17] I. Atomic and E. Agency, "Characteristics and use of Gadolinia fuels," *Int. At. Energy Agency*, 1995.

[18] J. Bruno, I. Casas, and I. Puigdomènech, "The kinetics of dissolution of UO2 under reducing conditions and the influence of an oxidized surface layer (UO2+x): Application of a continuous flow-through reactor," *Geochim. Cosmochim. Acta*, vol. 55, pp. 647–658, 1990, doi: 10.1016/0016-7037(91)90330-8.

[19] J. B. Joan de Pablo, Ignasi Casas, Javier Giménez, Frederic Clarens, Lara Duro, "The oxidative dissolution mechanism of uranium dioxide. The effect of pH and Oxygen Partial Pressure," vol. 807, no. 1, pp. 1–6, 2004.

[20] D. Pablo, I. Casas, J. Giménez, and C. Valle, "The oxidative dissolution mechanism of uranium dioxide . I . The effect of temperature in hydrogen carbonate medium," vol. 63, no. 19, pp. 3097–3103, 1999.

[21] A. N. Liu *et al.*, “Influence of Gd Doping on the Structure and Electrochemical Behavior of UO2,” *Electrochim. Acta*, 2017, doi: 10.1016/j.electacta.2017.07.006.
[22] A. B. Fidalgo and M. Jonsson, “Radiation induced dissolution of (U , Gd) O 2 pellets in aqueous solution e A comparison to standard UO 2 pellets,” *J. Nucl. Mater.*, vol. 514, pp. 216–223, 2019, doi: 10.1016/j.jnucmat.2018.11.037.
[23] A. Casella, B. Hanson, and W. Miller, “The effect of fuel chemistry on UO 2 dissolution *,” *J. Nucl. Mater.*, vol. 476, pp. 45–55, 2016, doi: 10.1016/j.jnucmat.2016.04.025.
[24] *Experimental methods of characterization 4*. 2018.
[25] J. Drenth, “X-ray Diffraction : Principles,” no. 1913, pp. 1–8, 2002.
[26] V. Accordingly and I. Boxes, *Principles of X-ray Diffraction*. 2006.
[27] R. Farre and M. J. Lagarda, “Properties and Determination ´ ,” pp. 1634–1639, 2003.
[28] P. Orientale and V. T. Michel, *8 - The Use of ICP-MS in Food Traceability*. Elsevier Ltd, 2016.
[29] M. Jaroniec, M. Kruk, and A. Sayari, *Adsorption methods for characterization of surface and structural properties of mesoporous molecular sieves*, vol. 117, no. 100. Elsevier Masson SAS, 1998.
[30] R. Wollast, “CHEMISTRY OF WEATHERING : Kinetics of the Surface-Controlled Dissolution of Oxide Minerals CaCO form 3 in the By integration,” no. 89, pp. 53–69, 1990.

Annex A: Experimental data

Experimental data used for the Figures in sections 5.2.1 and 5.2.2. are summarized below:

Table 1.A. Dissolution rate values of uranium in Reactor A.

pH	r (U) [mol/s·m^2]	Log (r) U
2,00	8,07(±0,66) ·10^{-10}	-9,09(±0,04)
8,2	2,54(±0,32) ·10^{-10}	-9,60(±0,06)
10,00	1,75(±0,26) ·10^{-10}	-9,76(±0,07)
12,00	2,68(±0,28) ·10^{-11}	-10,57(±0,05)
13,00	6,66(±0,80) ·10^{-12}	-11,18(±0,05)

Table 2.A. Dissolution rate values of uranium in Reactor B.

pH	r (U) [mol/s·m^2]	Log (r) U
2,00	6,70(±1,10) ·10^{-10}	-9,17(±0,07)
8,2	1,83(±0,17) ·10^{-11}	-10,74(±0,04)
10,00	1,28(±0,16) ·10^{-11}	-10,89(±0,06)
12,00	7,55(±0,65) ·10^{-12}	-11,12(±0,04)
13,00	1,13(±0,15) ·10^{-11}	-10,95(±0,09)

Table 3.A. Dissolution rate values of uranium in Reactor C.

pH	r (U) [mol/s·m^2]	Log (r) U
2,00	6,49(±0,92) ·10^{-10}	-9,19(±0,06)
8,2	7,56(±0,32) ·10^{-12}	-11,12(±0,05)
10,00	3,91(±0,49) ·10^{-12}	-11,41(±0,06)
12,00	5,50(±0,52) ·10^{-12}	-11,26(±0,04)
13,00	2,09(±0,29) ·10^{-11}	-10,68(±0,06)

Table 4.A. Dissolution rate values of gadolinium in Reactor B.

pH	r (Gd) [mol/s·m^2]	Log (r) Gd
2,00	1,43(±0,19) ·10^{-09}	-8,84(±0,06)
8,2	2,06(±0,22) ·10^{-10}	-9,69(±0,05)
10,00	1,25(±0,24) ·10^{-10}	-9,90(±0,09)
12,00	3,13(±0,12) ·10^{-11}	-10,50(±0,02)
13,00	4,19(±0,26) ·10^{-12}	-11,38(±0,03)

Table 5.A. Dissolution rate values of gadolinium in Reactor C.

pH	r (Gd) [mol/s·m^2]	Log (r) Gd
2,00	1,10(±0,01) ·10^{-09}	-8,96(±0,03)
8,2	3,23(±0,34) ·10^{-10}	-9,49(±0,05)
10,00	3,53(±0,36) ·10^{-10}	-9,45(±0,04)
12,00	4,10(±0,14) ·10^{-12}	-11,39(±0,10)
13,00	6,38(±0,87) ·10^{-13}	-12,20(±0,10)